MOX–Report No. 45/2014

An orthotropic active-strain model for the myocardium mechanics and its numerical approximation

Pezzuto, s.; Ambrosi,D.; Quarteroni, A.

MOX, Dipartimento di Matematica "F. Brioschi"
Politecnico di Milano, Via Bonardi 9 - 20133 Milano (Italy)

mox@mate.polimi.it http://mox.polimi.it

An orthotropic active–strain model for the myocardium mechanics and its numerical approximation

S. Pezzuto[a,c], D. Ambrosi[a], A. Quarteroni[b,a]

[a] *MOX–Dipartimento di Matematica, Politecnico di Milano, piazza Leonardo da Vinci 32, 20133 Milano, Italy*
[b] *École Polytechnique Fédérale de Lausanne, MATHICSE-CMCS, 1015 Lausanne, Switzerland*
[c] *Simula Research Laboratory, 1325 Lysaker, Norway*

Abstract

In the wide literature devoted to the cardiac structural mechanics, the strain energy proposed by Holzapfel and Ogden exhibits a number of interesting features: it has suitable mathematical properties and it is based on few material parameters that can, in principle, be identified by standard laboratory tests. In this work we illustrate the implementation of a numerical solver based on such a model for both the passive and active mechanics of the heart. Moreover we discuss its performance on a few tests that can be regarded as preliminary to the adoption of the Holzapfel–Ogden model for a real cardiac simulation.

While the passive behavior of the cardiac muscle is modeled as an orthotropic hyperelastic material, the active contraction is here accounted for a multiplicative decomposition of the deformation gradient, yielding the so–called "active strain" approach, a formulation that automatically preserves the ellipticity of the stress tensor and introduces just one extra parameter in the model.

We adopt the usual volumetric–isochoric decomposition of the stress tensor to obtain a mathematically consistent quasi–incompressible version of the material, then the numerical approximation applies to a classical Hu–Washizu three fields formulation. After introduction of the tangent problem, we select suitable finite element spaces for the representation of the physical fields. Boundary conditions are prescribed by introduction of a Lagrange multiplier.

The robustness and performance of the numerical solver are tested versus a novel benchmark test, for which an exact solution is provided. The curvature data obtained from the free contraction of muscular thin films are used to fit the active contraction parameter.

Introduction

Looking at the heart from a structural point of view, the myocardium can be considered as an hyperelastic orthotropic material, mechanically characterized by two families of mutually orthogonal directions, the fibers and the sheets. In the filling phase of the cardiac cycle, its chambers deform passively because of the venous pressure difference and the suction due to the release of elastic strain energy; in systole the fibers contract, actively produce a strain of the cardiac wall that by contracting the left ventricle determine the ejection of blood through the tricuspid aortic valve.

Among the many material models proposed in the literature, the hyperelastic strain energy model proposed by Holzapfel and Ogden (2009) to describe the mechanics of the passive myocardium is gaining an increasing popularity. Its simple invariant–based formulation and the small set of material parameters invoked makes it particularly attractive. Even more important, the material parameters of the model can,

Email addresses: simonep@simula.no (S. Pezzuto), davide.ambrosi@polimi.it (D. Ambrosi), alfio.quarteroni@epfl.ch (A. Quarteroni)

in principle, be determined on the basis of standard biaxial stress–strain tests (Göktepe et al., 2011; Wang et al., 2013a) without an *ad hoc* fitting in the specific application. While very recent papers have already addressed the use of this model to real geometry simulations (Wang et al., 2013b; Nobile et al., 2012; Rossi et al., 2012), a detailed discussion about the numerical implementation aspects and the performance of the model in test cases is still missing.

In this work we illustrate a step by step implementation of the Holzapfel–Ogden model in a finite element code, where the contractile ability of the muscle is accounted for an active strain approach. In particular, we address some issues that are sometimes overlooked in the literature: the codification of the active contraction in the model, the explicit calculation of the tangent problem, the efficient implementation of boundary conditions. The numerical code is then tested on a new benchmark of homogeneous (non–trivial) deformation, for which we provide a semi–explicit solution (up to an algebraic equation). The same test case where the distribution of the fibers orientation is variable in space points out the role of the fibers in dictating the cardiac rotation. The activation of the myocardium introduces, in our modeling framework, only one activation parameter and, coherently with the methodology that characterizes the passive mechanics, we fix such a parameter by an independent lab test. In particular, we fix the activation parameter γ at the value that predicts the correct bending produced by an activated monolayer of cardiomyocytes (Böl et al., 2009; Alford et al., 2010).

1. Background and notation

Given a body $\mathfrak{B}$ that is modeled as a continuum, we consider a reference configuration χ_0, and a generally unknown actual configuration χ as functions from $\mathfrak{B}$ to $\mathbb{R}^3$. The reference and actual placements of the body in $\mathbb{R}^3$ are $\Omega_0 := \chi_0(\mathfrak{B})$ and $\Omega := \chi(\mathfrak{B})$, respectively; given $\mathfrak{p} \in \mathfrak{B}$, $\mathbf{X} = \chi_0(\mathfrak{p}) \in \Omega_0$, and $\mathbf{x} = \chi(\mathfrak{p}) \in \Omega$, so that a deformation is a map:

$$\boldsymbol{\varphi} = \chi \circ \chi_0^{-1}, \qquad \boldsymbol{\varphi}\colon \Omega_0 \ni \mathbf{X} \mapsto \mathbf{x} = \chi\big(\chi_0^{-1}(\mathbf{X})\big) \in \Omega.$$

We assume $\boldsymbol{\varphi}$ to be a diffeomorphism from Ω_0 into Ω, whose derivative is the tensor gradient of deformation:

$$\mathsf{F}(\mathbf{X}) := \frac{\partial \boldsymbol{\varphi}}{\partial \mathbf{X}}, \qquad [\mathsf{F}_{ij}] = \frac{\partial \varphi_i}{\partial X_j}, \qquad i,j \in \{1,2,3\}.$$

Denoting by $\mathrm{Lin}^+(\mathbb{R}^3)$ the vector space of all linear transformations from $\mathbb{R}^3$ to $\mathbb{R}^3$ with strictly positive determinant, we define the set of admissible configurations as follows:

$$\mathscr{C} = \Big\{ \boldsymbol{\varphi}\colon \Omega_0 \to \Omega \text{ such that } \mathsf{F}(\mathbf{X}) \in \mathrm{Lin}^+ \text{ and } \boldsymbol{\varphi}|_{\partial_{\mathrm{D}}\Omega_0} = \mathbf{X} + \mathbf{g} \Big\}, \tag{1}$$

where $\mathbf{g}$ is a given displacement. In what follows we further assume that $\partial_{\mathrm{D}}\Omega_0$ and $\partial_{\mathrm{N}}\Omega_0$ are open subsets (with respect to the induced topology) of the boundary $\partial\Omega_0$ on which essential (Dirichlet) and natural (Neumann) boundary conditions apply, respectively.

As usual, we define the left and right Cauchy–Green and Green strain tensors as follows:

$$\mathsf{C} := \mathsf{F}^{\mathsf{T}}\mathsf{F}, \qquad \mathsf{B} := \mathsf{F}\mathsf{F}^{\mathsf{T}}, \qquad \text{and} \qquad \mathsf{E} := \frac{1}{2}\big(\mathsf{C} - \mathsf{I}\big),$$

respectively.

The constitutive relationship is prescribed within the hyperelasticity framework; this means that it exists a function $\mathcal{W}\colon \Omega_0 \times \mathrm{Lin}^+ \to \mathbb{R}$, called strain energy density function, which is objective, i.e.

$$\mathcal{W}(\mathbf{X}, \mathsf{F}) = \mathcal{W}(\mathbf{X}, \mathsf{Q}\mathsf{F}), \qquad \text{for all } \mathsf{Q} \in \mathrm{Orth}.$$

A natural way to automatically satisfy objectivity is to prescribe a function $\widehat{\mathcal{W}}\colon \Omega_0 \times \mathrm{Sym}^+ \to \mathbb{R}$ and then set $\mathcal{W}(\mathbf{X}, \mathsf{F}) = \widehat{\mathcal{W}}(\mathbf{X}, \mathsf{F}^{\mathsf{T}}\mathsf{F}) = \widehat{\mathcal{W}}(\mathbf{X}, \mathsf{C})$.

The Cauchy stress tensor is $\mathsf{T} = (\det \mathsf{F})^{-1}\mathsf{P}\mathsf{F}^{\mathsf{T}} = (\det \mathsf{F})^{-1}\mathsf{F}\mathsf{S}\mathsf{F}^{\mathsf{T}}$, where the first and the second Piola–Kirchhoff tensors, respectively P and S, are as follows

$$\mathsf{P} := \frac{\partial \mathcal{W}}{\partial \mathsf{F}}, \qquad \mathsf{S} := 2\frac{\partial \widehat{\mathcal{W}}}{\partial \mathsf{C}}. \tag{2}$$

For an hyperelastic material, the elastic equilibrium can be characterized as a minimization problem:

$$\min_{\mathbf{u}\in V} \left\{ \int_{\Omega_0} \widehat{\mathcal{W}}(\mathbf{X}, \mathsf{C})\, \mathrm{d}V - \left\langle \mathbf{f}^{\mathsf{ext}}, \mathbf{u} \right\rangle \right\} \tag{3}$$

where $\mathbf{u} := \boldsymbol{\varphi} - \mathbf{X}$ is the displacement and $\mathbf{f}^{\mathsf{ext}}$ is the linear functional which encodes for the external contributions. We need some extra restriction on the deformations and the functional itself, in order to establish that at least a minimum exists. A typical choice of the function space is $V := \mathscr{C} \cap \mathrm{W}^{1,s}(\Omega_0; \mathbb{R}^3)$, with $s > \frac{3}{2}$, $\frac{1}{s} + \frac{1}{q} < \frac{4}{3}$, and q such that $\operatorname{cof} \mathsf{F} \in \mathrm{L}^q(\Omega_0; \mathrm{Lin}^+)$, while the polyconvexity of the strain energy density function is generally a basic ingredient for the well–posedness of the minimization problem (Hughes and Marsden, 1994; Antman, 2005).

2. Passive mechanics

Given an hyperelastic material with strain energy function $\widehat{\mathcal{W}}(\mathbf{X}, \mathsf{C})$, we suppose that, for a fixed point $\mathbf{X} \in \Omega_0$, the following local invariance property is verified:

$$\widehat{\mathcal{W}}(\mathsf{C}) = \widehat{\mathcal{W}}(\mathsf{Q}\mathsf{C}\mathsf{Q}^{\mathsf{T}}), \qquad \text{for every } \mathsf{Q} \in \mathscr{G} \subseteq \mathrm{Orth}.$$

This relation means that the strain energy is the same if we change the reference configuration through the rotation Q, for any given deformation C (and so is the elastic response of the considered material). It is possible to show that $\mathscr{G}$ is a subgroup of Orth, with respect to the usual composition law. In particular, if $\mathscr{G} \equiv \mathrm{Orth}$, the material is *isotropic*; on the other hand, if $\mathscr{G}$ is a proper subgroup of Orth, the material is *anisotropic*.

Given an orthonormal ternary $\{\mathbf{f}_\circ, \mathbf{s}_\circ, \mathbf{n}_\circ\}$, in the reference configuration, for an *orthotropic* material the strain energy is invariant with respect to rotations around any versor of the triplet. This defines (Liu, 1982):

$$\mathscr{G}_{\mathsf{orth}} = \left\{ \mathsf{Q} \in \mathrm{Orth} \colon \mathsf{Q}(\mathbf{m} \otimes \mathbf{m})\mathsf{Q}^{\mathsf{T}} = \mathbf{m} \otimes \mathbf{m}, \text{ for } \mathbf{m} \in \{\mathbf{f}_\circ, \mathbf{s}_\circ, \mathbf{n}_\circ\} \right\}.$$

In our specific case, $\mathbf{f}_\circ$ represents the local muscle fiber direction, while $\mathbf{s}_\circ$ lies within the sheet and is orthogonal to $\mathbf{f}_\circ$. The last versor $\mathbf{n}_\circ = \mathbf{f}_\circ \wedge \mathbf{s}_\circ$ is the normal of the local sheet.

If a function $\widehat{\mathcal{W}}(\mathsf{C})$, with $\mathsf{C} \in \mathrm{Sym}^+$, is invariant with respect to $\mathscr{G}_{\mathsf{orth}}$, then there exists a representation $\widehat{\mathcal{W}}_{\mathsf{orth}}$ such that:

$$\widehat{\mathcal{W}}(\mathsf{C}) = \widehat{\mathcal{W}}_{\mathsf{orth}}(\mathsf{C}, \mathbf{f}_\circ \otimes \mathbf{f}_\circ, \mathbf{s}_\circ \otimes \mathbf{s}_\circ, \mathbf{n}_\circ \otimes \mathbf{n}_\circ),$$

for every $\mathsf{C} \in \mathrm{Sym}^+$ and with $\widehat{\mathcal{W}}_{\mathsf{orth}}$ isotropic with respect to its arguments. As a matter of fact, the dependency on $\mathbf{n}_\circ \otimes \mathbf{n}_\circ$ is redundant, because:

$$\mathbf{f}_\circ \otimes \mathbf{f}_\circ + \mathbf{s}_\circ \otimes \mathbf{s}_\circ + \mathbf{n}_\circ \otimes \mathbf{n}_\circ = \mathsf{I}.$$

The function $\widehat{\mathcal{W}}_{\mathsf{orth}}$ can be further specified by accounting for the isotropy requirement with respect to its tensor arguments. The Cayley–Hamilton theorem and the following observation:

$$(\mathbf{a} \otimes \mathbf{b})^k = (\mathbf{a} \cdot \mathbf{b})^{k-1}\mathbf{a} \otimes \mathbf{b}, \qquad \text{with } k > 0,$$

restrict the number of possible combinations. Observing that $\mathbf{n}_\circ$ is redundant and $\mathbf{f}_\circ$ and $\mathbf{s}_\circ$ are mutually orthogonal, we have that the invariant set for an orthotropic material is defined as follows:

$$\Upsilon_{\mathsf{orth}} = \left\{ \operatorname{tr} \mathsf{C},\ \operatorname{tr} \mathsf{C}^2,\ \operatorname{tr} \mathsf{C}^3,\ \mathbf{f}_\circ \cdot \mathsf{C}\mathbf{f}_\circ,\ \mathbf{s}_\circ \cdot \mathsf{C}\mathbf{s}_\circ,\ \mathbf{f}_\circ \cdot \mathsf{C}^2\mathbf{f}_\circ,\ \mathbf{s}_\circ \cdot \mathsf{C}^2\mathbf{s}_\circ \right\}. \tag{4}$$

It is actually possible to prove that only six of these seven invariants are independent, hence the set is not irreducible (Shariff, 2013).

The strain energy proposed in Holzapfel and Ogden (2009) is based on the following reduced set of invariants:

$$\Upsilon_{\mathsf{HO}} = \Big\{\mathcal{I}_1,\, \mathcal{I}_{4,\mathbf{f}_\circ},\, \mathcal{I}_{4,\mathbf{s}_\circ},\, \mathcal{I}_{8,\mathbf{f}_\circ\mathbf{s}_\circ}\Big\}, \tag{5}$$

where:

$$\mathcal{I}_1(\mathsf{C}) = \operatorname{tr}\mathsf{C}, \qquad \mathcal{I}_{4,\mathbf{a}}(\mathsf{C}) = \mathbf{a}\cdot\mathsf{C}\mathbf{a}, \qquad \mathcal{I}_{8,\mathbf{ab}}(\mathsf{C}) = \mathbf{a}\cdot\mathsf{C}\mathbf{b}.$$

The material is assumed to be incompressible, thus $\operatorname{tr}\mathsf{C}^3$ can be represented as a function of the first and second invariant of C through the Cayley–Hamilton theorem. Moreover, the dependency on the quadratic terms is (partially) expressed by $\mathcal{I}_{8,\mathbf{f}_\circ\mathbf{s}_\circ}$, thanks to a relationship can be established between the invariants (Merodio and Ogden, 2006).

From a kinematic viewpoint, all the invariants have a clear interpretation: for instance, $\mathcal{I}_{4,\mathbf{a}}$ is the square of the local stretch along the direction $\mathbf{a}$, while $\mathcal{I}_{8,\mathbf{ab}}$ is related to the angle spanned by the vectors $\mathsf{F}\mathbf{a}$ and $\mathsf{F}\mathbf{b}$, in the actual configuration, supposing that $\mathbf{a}$ and $\mathbf{b}$ are initially orthogonal.

A further hypothesis is the additive splitting of the strain energy, that separates the contributions of each specific deformation measure to the total energy:

$$\begin{aligned}\widehat{\mathcal{W}}(\mathsf{C}) &= \widetilde{\mathcal{W}}(\mathcal{I}_1, \mathcal{I}_{4,\mathbf{f}_\circ}, \mathcal{I}_{4,\mathbf{s}_\circ}, \mathcal{I}_{8\mathbf{f}_\circ\mathbf{s}_\circ}) \\ &= \widetilde{\mathcal{W}}_1(\mathcal{I}_1) + \widetilde{\mathcal{W}}_{4,\mathbf{f}_\circ}(\mathcal{I}_{4,\mathbf{f}_\circ}) + \widetilde{\mathcal{W}}_{4,\mathbf{s}_\circ}(\mathcal{I}_{4,\mathbf{s}_\circ}) + \widetilde{\mathcal{W}}_{8,\mathbf{f}_\circ\mathbf{s}_\circ}(\mathcal{I}_{8,\mathbf{f}_\circ\mathbf{s}_\circ}).\end{aligned} \tag{6}$$

Besides its mathematical convenience, this splitting allows an easy identification of the corresponding material parameters from an experiment, because each term has its precise physical meaning.

The exponential form of each term in the strain energy (6) accommodates the typical response of a biological tissue, according to which the greater the strain, the greater the apparent stiffness:

$$\widetilde{\mathcal{W}}_1(\mathcal{I}_1) = \frac{a}{2b}\Big[e^{b(\mathcal{I}_1-3)} - 1\Big],$$

$$\widetilde{\mathcal{W}}_{4,\mathbf{f}_\circ}(\mathcal{I}_{4,\mathbf{f}_\circ}) = \frac{a_\mathsf{f}}{2b_\mathsf{f}}\Big[e^{b_\mathsf{f}(\mathcal{I}_{4,\mathbf{f}_\circ}-1)_+^2} - 1\Big],$$

$$\widetilde{\mathcal{W}}_{4,\mathbf{s}_\circ}(\mathcal{I}_{4,\mathbf{s}_\circ}) = \frac{a_\mathsf{s}}{2b_\mathsf{s}}\Big[e^{b_\mathsf{s}(\mathcal{I}_{4,\mathbf{s}_\circ}-1)_+^2} - 1\Big],$$

$$\widetilde{\mathcal{W}}_{8,\mathbf{f}_\circ\mathbf{s}_\circ}(\mathcal{I}_{8,\mathbf{f}_\circ\mathbf{s}_\circ}) = \frac{a_\mathsf{fs}}{2b_\mathsf{fs}}\Big[e^{b_\mathsf{fs}\mathcal{I}_{8,\mathbf{f}_\circ\mathbf{s}_\circ}^2} - 1\Big],$$

where $g(x)_+ := \max\{g(x), 0\}$ is the positive part of $g(x)$.

Thanks to (2) we can compute the explicit form of the Cauchy stress tensor T,

$$\begin{aligned}\mathsf{T} &= ae^{b(\mathcal{I}_1-3)}\mathsf{B} - p\mathsf{I} \\ &+ 2\,a_\mathsf{f}(\mathcal{I}_{4,\mathbf{f}_\circ}-1)_+ e^{b_\mathsf{f}(\mathcal{I}_{4,\mathbf{f}_\circ}-1)_+^2}\,\mathbf{f}\otimes\mathbf{f} + 2\,a_\mathsf{s}(\mathcal{I}_{4,\mathbf{s}_\circ}-1)_+ e^{b_\mathsf{s}(\mathcal{I}_{4,\mathbf{s}_\circ}-1)_+^2}\,\mathbf{s}\otimes\mathbf{s} \\ &+ a_\mathsf{fs}\mathcal{I}_{8,\mathbf{f}_\circ\mathbf{s}_\circ} e^{b_\mathsf{fs}\mathcal{I}_{8,\mathbf{f}_\circ\mathbf{s}_\circ}^2}\,(\mathbf{f}\otimes\mathbf{s} + \mathbf{s}\otimes\mathbf{f}),\end{aligned} \tag{7}$$

where the Lagrange multiplier p enforces incompressibility, $\mathbf{f} = \mathsf{F}\mathbf{f}_\circ$ and $\mathbf{s} = \mathsf{F}\mathbf{s}_\circ$. The transversely isotropic version of this model can be formally recovered taking $a_\mathsf{s} = b_\mathsf{s} = a_\mathsf{fs} = b_\mathsf{fs} = 0$, while the isotropic one corresponds to assume also $a_\mathsf{f} = b_\mathsf{f} = 0$; furthermore, in these two cases the set of invariants is smaller than the irreducible one, always because the quadratic terms are not considered.

It's interesting to observe that the assumptions made on the symmetry of the material, and in particular on its microstructure, reflect in the tensorial form of the Cauchy stress tensor: the isotropic contribution can be thought as due to the extracellular matrix, while the anisotropic terms play a role along the fibers and the sheets, or when the deformation changes the angle between the two.

As could be expected for physical and mathematical reasons, the predictions of the model (7) in the compressive regime would be incorrect because fibers do not support compressive loads. For this reason Holzapfel and Ogden suggest that the anisotropic terms associated to $\mathcal{I}_{4,\mathbf{f}_\circ}$ and $\mathcal{I}_{4,\mathbf{s}_\circ}$ are turned off under compression, i.e. when $\mathcal{I}_{4,\mathbf{f}_\circ} \leq 1$, or $\mathcal{I}_{4,\mathbf{s}_\circ} \leq 1$, respectively.

An interesting property of this formulation is that $\widetilde{\mathcal{W}}_{4,\cdot}$ is strongly convex.

2.1. Quasi–incompressible formulation

Following a common approach in soft tissue mechanics, the Holzapfel–Ogden model assumes that the myocardium is an incompressible material; the usual argument in this respect is that biological tissues are mostly made of water, an incompressible fluid. Nonetheless, a living tissue is not just a vesicle filled with water, it is rather an intricate bundle of various cells, vessels of different size, collagen, elastin, other substances that compose the extracellular matrix, and perfused blood; the latter in particular is responsible for the large volume variation (up to 30%) observed in the ventricle (Yin et al., 1996). Concluding, even neglecting the role of perfused blood, an extra degree of freedom that takes into the account very moderate volumetric changes, is not excluded by experimental evidence. But, more importantly, there are numerical advantages brought by a quasi–incompressible formulation over an incompressible one (Simo and Taylor, 1991).

For a given incompressible model, such us the Holzapfel–Ogden's one, a quasi–incompressible version can be derived by introducing the following multiplicative decomposition of the deformation gradient tensor:

$$\mathsf{F} = \mathsf{F}_{\mathsf{iso}}\mathsf{F}_{\mathsf{vol}}, \tag{8}$$

that is, by considering the local deformation as the composition of purely volumetric deformation, followed by an isochoric one. In particular, we would like to have that $\det \mathsf{F}_{\mathsf{iso}} = 1$ and $\mathsf{F}_{\mathsf{vol}} = \alpha\mathsf{I}$, so:

$$J = \det \mathsf{F} = \det \mathsf{F}_{\mathsf{iso}} \cdot \det \mathsf{F}_{\mathsf{vol}} = \alpha^3, \qquad \text{so} \qquad \alpha = J^{\frac{1}{3}}.$$

Within this context, the two deformations $\mathsf{F}_{\mathsf{iso}}$ and $\mathsf{F}_{\mathsf{vol}}$ (which is just J times the identity tensor) contribute additively to the strain energy, so:

$$\mathcal{W}(\mathsf{F}) = \mathcal{W}_{\mathsf{iso}}(\mathsf{F}_{\mathsf{iso}}) + \mathcal{W}_{\mathsf{vol}}(J). \tag{9}$$

The splitting can be applied to any strain energy for an incompressible material and, in this work, $\mathcal{W}_{\mathsf{iso}}(\mathsf{F}_{\mathsf{iso}})$ takes the form of the Holzapfel–Ogden model.

The second term of the r.h.s. of (9) is the volumetric energy, and it increases when $J \neq 1$. Several forms for $\mathcal{W}_{\mathsf{vol}}$ can be found in the literature: as a guiding principle, a good choice is a function bounded from below, convex, and whose first and second derivative for $J = 1$ are respectively zero. In general, one would expect that $\mathcal{W}_{\mathsf{iso}} \to \infty$ as $J \to 0$ and $J \to \infty$, because from a physical viewpoint we are compressing the body down to a point or dilating it indefinitely. Nevertheless, we are considering a quasi–incompressible model, and we expect to keep $J \approx 1$, so practically there is no difference between the many models present in the literature from a practical viewpoint; at the mathematical level instead, the well–posedness of the problem can be compromised in some cases (Schröder and Neff, 2003). In our simulation we use

$$\mathcal{W}_{\mathsf{vol}}(J) = \frac{\kappa}{4}\big(J^2 - 1 - 2\ln J\big),$$

where $\kappa \gg 1$ is the bulk modulus. We remark that $\mathcal{W}'_{\mathsf{vol}}(1) = 0$ and $\mathcal{W}''_{\mathsf{vol}}(1) = \kappa$.

The Cauchy stress tensor is obtained by means of a Piola transformation and relation (2):

$$\mathsf{T} = \mathsf{T}_{\mathsf{iso}} + \mathsf{T}_{\mathsf{vol}} = \operatorname{dev} \overline{\mathsf{T}}_{\mathsf{iso}} + \mathcal{W}'_{\mathsf{vol}}(J)\mathsf{I} \tag{10}$$

where $\overline{\mathsf{T}}_{\mathsf{iso}}$ is the fictitious Cauchy stress tensor associated to the strain energy $\mathcal{W}_{\mathsf{iso}}$. In particular, for the Holzapfel–Ogden model, we can just substitute (7) by $J\overline{\mathsf{T}}_{\mathsf{iso}}$:

$$\begin{aligned} J\overline{\mathsf{T}}_{\mathsf{iso}} = {} & a e^{b(\mathcal{I}_1 - 3)}\mathsf{B}_{\mathsf{iso}} \\ & + 2\,a_{\mathsf{f}}(\mathcal{I}^{\mathsf{iso}}_{4,\mathbf{f}_\circ} - 1)_+ e^{b_{\mathsf{f}}(\mathcal{I}^{\mathsf{iso}}_{4,\mathbf{f}_\circ} - 1)^2_+}\,\mathbf{f}_{\mathsf{iso}} \otimes \mathbf{f}_{\mathsf{iso}} + 2\,a_{\mathsf{s}}(\mathcal{I}^{\mathsf{iso}}_{4,\mathbf{s}_\circ} - 1)_+ e^{b_{\mathsf{s}}(\mathcal{I}^{\mathsf{iso}}_{4,\mathbf{s}_\circ} - 1)^2_+}\,\mathbf{s}_{\mathsf{iso}} \otimes \mathbf{s}_{\mathsf{iso}} \\ & + a_{\mathsf{fs}}\mathcal{I}^{\mathsf{iso}}_{8,\mathbf{f}_\circ\mathbf{s}_\circ} e^{b_{\mathsf{fs}}(\mathcal{I}^{\mathsf{iso}}_{8,\mathbf{f}_\circ\mathbf{s}_\circ})^2}\,(\mathbf{f}_{\mathsf{iso}} \otimes \mathbf{s}_{\mathsf{iso}} + \mathbf{s}_{\mathsf{iso}} \otimes \mathbf{f}_{\mathsf{iso}}), \end{aligned}$$

where all the quantities marked with either superscript $(\circ)^{\mathsf{iso}}$ or subscript $(\circ)_{\mathsf{iso}}$ have to be computed with respect to $\mathsf{F}_{\mathsf{iso}}$ instead of F. Observe also that the pressure is exactly $-\mathcal{W}'_{\mathsf{vol}}(J)$.

3. Active contraction

During an isometric test, an electrically stimulated cardiomyocyte kept at fixed length produces an active force. On the other hand, an opposition force is measured also when the cell is stretched over its resting length without electric stimulus, as an elastic response: this is just a passive force. It is therefore natural to assume that the total force exerted by the cell can be decomposed into two distinct contributions (Wakatsuki et al., 2000): a passive one, that represents the elastic response of the material to external loads, when no active contraction is involved, and an active contribution that encodes the forces generated at the microscale:

$$f_{\mathsf{total}} = f_{\mathsf{active}} + f_{\mathsf{passive}}. \tag{11}$$

Suppose now that the mechanical properties of a myocyte can be described by an hyperelastic material with strain energy density function $\mathcal{W}\colon \mathrm{Lin}^+ \to \mathbb{R}^+$. Then, the Cauchy stress is:

$$\mathsf{T} = (\det \mathsf{F})^{-1} \frac{\partial \mathcal{W}}{\partial \mathsf{F}} \mathsf{F}^{\mathsf{T}}. \tag{12}$$

This stress is purely passive, so it ideally accounts for f_{passive}. When the activation is involved, an extra term shows up, associated to f_{active}:

$$\mathsf{T}(\mathsf{F}, \xi) = \mathsf{T}_{\mathsf{e}}(\mathsf{F}) + \mathsf{T}_{\mathsf{a}}(\mathsf{F}, \xi) = (\det \mathsf{F})^{-1} \frac{\partial \mathcal{W}}{\partial \mathsf{F}} \mathsf{F}^{\mathsf{T}} + \mathsf{T}_{\mathsf{a}}(\mathsf{F}, \xi).$$

The active stress T_{a} depends on some internal variable ξ, that encodes the biochemical status of the cell and, in general, is a function of the deformation gradient F. This dependence is reported for single cardiomyocytes Iribe et al. (2007) and, in a continuum mechanics framework, also follows from physical considerations (a force per unit area changes value when the area changes).

The specific tensorial form of T_{a} can be deduced enforcing the correct symmetries from the microstructure and objectivity. The 2$^{\text{nd}}$ Piola–Kirchhoff tensor associated to T_{a} reads:

$$\mathsf{S}_{\mathsf{a}}(\mathsf{F}, \xi) = (\det \mathsf{F}) \mathsf{F}^{-1} \mathsf{T}_{\mathsf{a}}(\mathsf{F}, \xi) \mathsf{F}^{-\mathsf{T}}.$$

The first requirement is objectivity, meaning that S_{a} depends on F only through U, where U is such that $\mathsf{F} = \mathsf{R}\mathsf{U}$. This is guaranteed if, for instance,

$$\mathsf{S}_{\mathsf{a}}(\mathsf{F}, \xi) = \widehat{\mathsf{S}}_{\mathsf{a}}(\mathsf{F}^{\mathsf{T}}\mathsf{F}, \xi) = \widehat{\mathsf{S}}_{\mathsf{a}}(\mathsf{C}, \xi).$$

The second requirement is that the active stress acts in the fiber direction $\mathbf{f}_\circ$, so we look for a transversely isotropic tensor $\widehat{\mathsf{S}}_{\mathsf{a}}$ of its variables C and ξ. Following what done in section 2, we obtain

$$\widehat{\mathsf{S}}_{\mathsf{a}}(\mathsf{C}, \xi) = s_1\, \mathsf{I} + s_2\, \mathsf{C} + s_4\, \mathbf{f}_\circ \otimes \mathbf{f}_\circ + s_5\, \mathrm{sym}(\mathsf{C}\mathbf{f}_\circ \otimes \mathbf{f}_\circ), \tag{13}$$

where s_1, s_2, s_4 and s_5 are scalar functions of ξ and the invariants

$$\Upsilon = \Big\{ \mathrm{tr}\, \mathsf{C}, \mathrm{tr}\, \mathsf{C}^2, \mathbf{f}_\circ \cdot \mathsf{C}\mathbf{f}_\circ, \mathbf{f}_\circ \cdot \mathsf{C}^2 \mathbf{f}_\circ \Big\},$$

and where we have assumed that $\det \mathsf{C} = 1$ and $\mathbf{f}_\circ \cdot \mathbf{f}_\circ = 1$. The functional dependence of (13) can be very complex; a common approach consists in simplifying it by neglecting the quadratic invariants, yielding

$$\widehat{\mathsf{S}}_{\mathsf{a}}(\mathsf{C}, \xi) = s_1(\mathcal{I}_1, \mathcal{I}_{4,\mathbf{f}_\circ}, \xi)\, \mathsf{I} + s_4(\mathcal{I}_1, \mathcal{I}_{4,\mathbf{f}_\circ}, \xi)\, \mathbf{f}_\circ \otimes \mathbf{f}_\circ. \tag{14}$$

Although simpler than (13), this form is much richer than what has been proposed over the last decades in the literature: the dependence on the invariant $\mathcal{I}_1$ is usually not considered in (14) and, most of the time, also s_1 is neglected, so that

$$\widehat{\mathsf{S}}_{\mathsf{a}}(\mathsf{C},\xi) = s_1(\mathcal{I}_{4,\mathbf{f}_\circ},\xi)\,\mathsf{I},$$

or, in terms of Cauchy stress,

$$\mathsf{T}_{\mathsf{a}}(\mathsf{F},\xi) = s_{\mathsf{a}}(\mathcal{I}_{4,\mathbf{f}_\circ},\xi)\,\mathsf{F}\mathbf{f}_\circ\otimes\mathsf{F}\mathbf{f}_\circ. \tag{15}$$

The active stress acts in the deformed fiber direction, with a magnitude that nonlinearly depends on the current stretch of the fibers. Some authors (Usyk et al., 2000; Aguado-Sierra et al., 2011) adopt an orthotropic active stress, which actually is a transversely isotropic activation of the form

$$\widehat{\mathsf{S}}_{\mathsf{a}}(\mathsf{C},\xi) = s_{\mathsf{a}}(\mathcal{I}_{4,\mathbf{f}_\circ},\xi)\,\mathbf{f}_\circ\otimes\mathbf{f}_\circ + r\,s_{\mathsf{a}}(\mathcal{I}_{4,\mathbf{f}_\circ},\xi)\,(\mathsf{I}-\mathbf{f}_\circ\otimes\mathbf{f}_\circ) \tag{16}$$

for some factor $r \geq 0$ (usually $0.2 \div 0.4$).

The functional dependence of the scalar factor s_{a} (a force per unit area) on the electrochemical signalling and on the strain is usually related to the active force generated by a single cardiomyocyte f_{active}, in order to fit the experimental data. A possible starting point is to be inspired by a specific test case such as the homogeneous contraction of an incompressible rod along its $\mathbf{f}_\circ$ axis:

$$\mathsf{F} = \lambda\mathbf{f}_\circ\otimes\mathbf{f}_\circ + \frac{1}{\sqrt{\lambda}}(\mathsf{I}-\mathbf{f}_\circ\otimes\mathbf{f}_\circ).$$

Substituting the latter into Equation (15) we have

$$\mathsf{T}_{\mathsf{a}}(\lambda,\xi) = s_{\mathsf{a}}(\lambda^2,\xi)\lambda^2\,\mathbf{f}_\circ\otimes\mathbf{f}_\circ = \frac{f_{\mathsf{active}}}{A_0}\lambda\,\mathbf{f}_\circ\otimes\mathbf{f}_\circ,$$

where A_0 is the initial cross sectional area. Simplifying we get

$$f_{\mathsf{active}}(\lambda,\xi) = \lambda s_{\mathsf{a}}(\lambda^2,\xi)A_0. \tag{17}$$

Therefore the force is independent on λ if (observe that $\lambda^2 = \mathcal{I}_{4,\mathbf{f}_\circ}$):

$$s_{\mathsf{a}}(\mathcal{I}_{4,\mathbf{f}_\circ},\xi) = \frac{f_{\mathsf{active}}(\xi)}{A_0\sqrt{\mathcal{I}_{4,\mathbf{f}_\circ}}}.$$

More physiologically motivated choices of s_{a} depend linearly on λ, in order to recover the Frank–Starling effect for moderate values of the strain. Another option is to use a nonlinear dependence such as $\lambda\exp(-\lambda^2)$ (or a quadratic approximation of it) which captures an optimal value of the sarcomere stretch and the descending limb of Frank–Starling relationship (Weiwad et al., 2000).

The construction of a specific form for the active stress term T_{a} is delicate, because it should account for the geometry of the deformation, which changes considerably in finite strain. Moreover, an important property of a stress–strain relationship, that holds also for an activated material, is that *an increase of the strain is accompanied by an increase of the stress, and vice–versa* (Baker and Ericksen, 1954; Hughes and Marsden, 1994), and translates in the positiveness of the derivative of f_{active} of equation (17)

$$\frac{1}{A_0}\frac{\partial f_{\mathsf{active}}}{\partial\lambda} = s_{\mathsf{a}}(\mathcal{I}_{4,\mathbf{f}_\circ},\xi) + 2\mathcal{I}_{4,\mathbf{f}_\circ}\frac{\partial s_{\mathsf{a}}(\mathcal{I}_{4,\mathbf{f}_\circ},\xi)}{\partial\mathcal{I}_{4,\mathbf{f}_\circ}} > 0. \tag{18}$$

This property does not apply to the (standing alone) active stress in any strain range, as the force produced by cardiomyocytes exhibits a maximum at a threshold strain. However the monotonicity (or strong ellipticity) must be satisfied by the *total* stress (active plus passive) to ensure the well–posedness of the mathematical problem (Ambrosi and Pezzuto, 2012).

An alternative approach, the so–called active strain, consists in assuming a multiplicative decomposition of the deformation gradient tensor

$$\mathsf{F} = \mathsf{F}_{\mathsf{e}}\mathsf{F}_{\mathsf{a}}$$

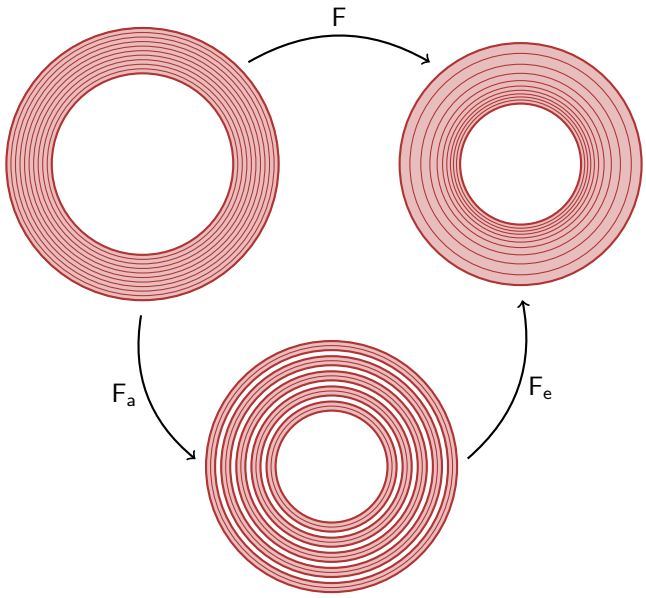

Figure 1: Pictorial view of the active strain approach.

in an elastic deformation F_e and an active distortion F_a.

The idea, sketched in figure 1, is the following: an inelastic process, dictated by the biochemistry, locally changes the length and the shape of the fibers, i.e. the tissue microstructure; then, an elastic deformation F_e accommodates these local changes in order to preserve the compatibility of the deformation F. The physiological basis behind this approach resides in the contractile units of the myocytes: the sarcomeres shorten because of the sliding filaments of the actin–myosin molecular motor, and this shortening is encoded by F_a, and the fictitious intermediate placement determined by F_a is the new reference configuration for the elastic deformation.

The strain energy density is a function of F_e only, the active deformation F_a being a fully dissipative process; the objective is to minimise the total elastic energy with respect to all the admissible configurations:

$$\min_{\mathbf{u}\in V}\left\{\int_{\Omega_0}\mathcal{W}(\mathsf{F}\mathsf{F}_\mathsf{a}^{-1})\,(\det\mathsf{F}_\mathsf{a})\,\mathrm{d}V-\left\langle\mathbf{f}^{\mathsf{ext}},\mathbf{u}\right\rangle\right\}. \tag{19}$$

If no dead–load is applied, i.e. $\mathbf{f}^{\mathsf{ext}}=0$, and no Dirichlet boundary conditions are enforced, then one could argue that $\mathsf{F}=\mathsf{F}_\mathsf{a}$, since $\mathsf{F}_\mathsf{e}=\mathsf{I}$ is a local minimum of $\mathcal{W}$ (actually, if $\mathcal{W}$ and V are convex, the minimum is global and hence unique). However, there is no guarantee that there exists a deformation $\boldsymbol{\varphi}$ such that $\textsc{Grad}\,\boldsymbol{\varphi}=\mathsf{F}_\mathsf{a}$. This restricts the set of possible solutions among which the minimization problem makes sense from a geometric viewpoint, and it yields a residual stress in the body, even when no body force or surface traction apply.

Suppose that a minimum exists; then, the first variation of the functional in (19) must be null for every admissible variation $\boldsymbol{\eta}_0\in\mathcal{T}_{\boldsymbol{\varphi}}\mathscr{C}\cap V$:

$$\int_{\Omega_0}(\det\mathsf{F}_\mathsf{a})\frac{\partial\mathcal{W}(\mathsf{F}_\mathsf{e})}{\partial\mathsf{F}_\mathsf{e}}\mathsf{F}_\mathsf{a}^{-\mathsf{T}}:\textsc{Grad}\,\boldsymbol{\eta}_0\,\mathrm{d}V-\left\langle\mathbf{f}^{\mathsf{ext}},\boldsymbol{\eta}_0\right\rangle=0.$$

The 1st Piola–Kirchhoff and the Cauchy stress tensors are, respectively:

$$\mathsf{P}=(\det\mathsf{F}_\mathsf{a})\frac{\partial\mathcal{W}(\mathsf{F}_\mathsf{e})}{\partial\mathsf{F}_\mathsf{e}}\mathsf{F}_\mathsf{a}^{-\mathsf{T}},\qquad\mathsf{T}=(\det\mathsf{F}_\mathsf{e})^{-1}\frac{\partial\mathcal{W}(\mathsf{F}_\mathsf{e})}{\partial\mathsf{F}_\mathsf{e}}\mathsf{F}_\mathsf{e}^{\mathsf{T}}.$$

If no activation is triggered, then $\mathsf{F}_\mathsf{a} = \mathsf{I}$, $\mathsf{F}_\mathsf{e} = \mathsf{F}$, and the passive behavior of the material is recovered. On the other hand, if $\mathsf{F} = \mathsf{I}$ and $\mathsf{F}_\mathsf{e} = \mathsf{F}_\mathsf{a}^{-1}$, the Cauchy stress tensor can be interpreted as a purely active response:

$$\mathsf{T} = (\det \mathsf{F}_\mathsf{a})\, \frac{\partial \mathcal{W}}{\partial \mathsf{F}_\mathsf{e}}\bigg|_{\mathsf{F}_\mathsf{e}=\mathsf{F}_\mathsf{a}^{-1}} \mathsf{F}_\mathsf{a}^{-\mathsf{T}}.$$

Interestingly, the tensorial form of this purely active response (and in absence of residual stress) cannot be straightforwardly deduced from F_a, as opposed to the active stress in (15): even in the case of F_a being a pure shortening in the fiber direction, say $\mathsf{F}_\mathsf{a} = (1-\gamma)\mathbf{f}_\circ \otimes \mathbf{f}_\circ$, in general the stress response occurs in any direction.

A physiologically motivated choice for F_a is transversely isotropic and locally isochoric tensor of the form

$$\mathsf{F}_\mathsf{a} = (1-\gamma)\mathbf{f}_\circ \otimes \mathbf{f}_\circ + \frac{1}{1-\gamma}(\mathsf{I} - \mathbf{f}_\circ \otimes \mathbf{f}_\circ), \tag{20}$$

as supported by the observation that during a contraction myocytes shorten in the sarcomeres direction and they don't change their volume significantly (Boyett et al., 1991).

The coefficient γ, which depends on the internal dynamics described by the some variable ξ (the action potential and/or specific ionic currents) in this bare–bones framework is not an explicit function of the apparent deformation F.

4. Numerical approximation

The numerical discretization of the equilibrium equations for a quasi–incompressible material is particularly delicate when κ is very large, i.e. when we try to enforce incompressibility: in this case the *locking* phenomenon might be observed. In such a regime a possible strategy is to go back to the full incompressible formulation, with the pressure as a Lagrange multiplier. The resulting formulation of the tangent problem, required by the Newton method, reads as a Stokes type problem, which introduces various difficulties from a computational viewpoint.

A widely accepted alternative, that preserves quasi–incompressibility while solving the "locking" issue, is the so called "three–fields" or "Hu–Washizu" formulation. The idea is to widen the number of unknowns of the problem and introduce the following generalized deformation gradient:

$$\tilde{\mathsf{F}}(\boldsymbol{\varphi}, \Theta) := \Theta^{\frac{1}{3}} (\det \mathsf{F})^{-\frac{1}{3}} \mathsf{F},$$

which is a function of the new independent variable $\Theta \in Q := \mathrm{L}^2(\Omega_0)$, with $\Theta > 0$. The strain energy density function will be a function $\mathcal{W}$ of $\tilde{\mathsf{F}}$, hence in particular of Θ and F through $\tilde{\mathsf{F}}$.

Now consider a quasi–incompressible formulation for $\mathcal{W}$. The first step is the splitting of $\tilde{\mathsf{F}}$ into its isochoric and volumetric parts:

$$\begin{aligned}
(\tilde{\mathsf{F}}(\boldsymbol{\varphi}, \Theta))_{\mathsf{vol}} &:= \det(\tilde{\mathsf{F}}(\boldsymbol{\varphi}, \Theta)) = \Theta, \\
(\tilde{\mathsf{F}}(\boldsymbol{\varphi}, \Theta))_{\mathsf{iso}} &:= (\tilde{\mathsf{F}}(\boldsymbol{\varphi}, \Theta))_{\mathsf{vol}}^{-\frac{1}{3}} \tilde{\mathsf{F}}(\boldsymbol{\varphi}, \Theta) = (\det \mathsf{F})^{-\frac{1}{3}} \mathsf{F} = \mathsf{F}_{\mathsf{iso}}.
\end{aligned}$$

The second step is the additive splitting of the energy:

$$\mathcal{W}(\tilde{\mathsf{F}}) = \mathcal{W}_{\mathsf{iso}}(\mathsf{F}_{\mathsf{iso}}) + \mathcal{W}_{\mathsf{vol}}(\Theta).$$

The last ingredient is to state a variational principle. Consider the following functional $\mathcal{F}_{\mathsf{HW}}$ of the variables $(\mathbf{u}, \Theta, p) \in V \times Q \times Q$:

$$\mathcal{F}_{\mathsf{HW}}(\mathbf{u}, \Theta, p) := \int_{\Omega_0} \left(\widehat{\mathcal{W}}_{\mathsf{iso}}(\mathbf{X}, \mathsf{C}_{\mathsf{iso}}) + \mathcal{W}_{\mathsf{vol}}(\mathbf{X}, \Theta) + p(J - \Theta) \right) \mathrm{d}V - \left\langle \mathbf{f}^{\mathsf{ext}}, \mathbf{u} \right\rangle, \tag{21}$$

where $\mathcal{F}^{\mathsf{ext}}$ encodes the work of external forces. $\mathcal{F}_{\mathsf{HW}}$ mimics the functional in (3) with the additional term $p(J - \Theta)$ that enforces the constraint $\Theta = J$. In this respect, p is the pressure.

Denoting with $\mathrm{D}_{\mathbf{u}}$ the partial Gâteaux derivative with respect to $\mathbf{u}$, we have

$$\begin{aligned}\langle \mathrm{D}_{\mathbf{u}}\mathcal{F}_{\mathsf{HW}}, \boldsymbol{\eta}_0\rangle &= \int_{\Omega_0} 2\mathsf{F}\,\textsc{Dev}\,\frac{\partial\widehat{\mathcal{W}}_{\mathsf{iso}}}{\partial\mathsf{C}_{\mathsf{iso}}} : \textsc{Grad}\,\boldsymbol{\eta}_0\,\mathrm{d}V + \int_{\Omega_0} p\,\mathrm{cof}\,\mathsf{F} : \textsc{Grad}\,\boldsymbol{\eta}_0\,\mathrm{d}V - \left\langle \mathbf{f}^{\mathsf{ext}}, \boldsymbol{\eta}_0\right\rangle \\ &= \int_{\Omega} \mathrm{dev}\,\overline{\mathsf{T}}_{\mathsf{iso}} : \nabla\boldsymbol{\eta}\,\mathrm{d}v + \int_{\Omega} p\,\mathrm{div}\,\boldsymbol{\eta}\,\mathrm{d}v - \left\langle \mathbf{f}^{\mathsf{ext}}, \boldsymbol{\eta}\right\rangle,\end{aligned}$$

where $\mathbf{f}^{\mathsf{ext}}$ is the linear functional in the actual configuration, $\textsc{Dev}\colon \mathsf{A} \mapsto J^{-\frac{2}{3}}\left(\mathsf{A} - \frac{1}{3}(\mathsf{C} : \mathsf{A})\mathsf{C}^{-1}\right)$ and $\mathrm{dev}\colon \mathsf{A} \mapsto \mathsf{A} - \frac{1}{3}\,\mathrm{tr}\,\mathsf{A}$. The corresponding Cauchy stress tensor is simply as follows:

$$\mathsf{T} = \mathrm{dev}\,\overline{\mathsf{T}}_{\mathsf{iso}} + p\mathsf{I}.$$

In order to fully characterize the minimum, we have two more derivatives to enforce, one with respect to Θ and the other to p:

$$\begin{aligned}\langle \mathrm{D}_{\Theta}\mathcal{F}_{\mathsf{HW}}, \Xi\rangle &= \int_{\Omega_0} \big(\mathcal{W}'_{\mathsf{vol}}(\Theta) - p\big)\Xi\,\mathrm{d}V = \int_{\Omega} \big(\mathcal{W}'_{\mathsf{vol}}(\Theta) - p\big)\Xi\,J^{-1}\mathrm{d}v, \\ \langle \mathrm{D}_{p}\mathcal{F}_{\mathsf{HW}}, q\rangle &= \int_{\Omega_0} q(J-\Theta)\,\mathrm{d}V = \int_{\Omega} q(J-\Theta)\,J^{-1}\mathrm{d}v.\end{aligned}$$

The final variational problem reads as follows:

$$\begin{aligned}&\text{Find } (\mathbf{u}, \Theta, p) \in V \times Q \times Q \text{ such that} \\ &\int_{\Omega}\Big(\mathrm{dev}\,\overline{\mathsf{T}}_{\mathsf{iso}} : \nabla\boldsymbol{\eta} + p\,\mathrm{div}\,\boldsymbol{\eta}\Big)\,\mathrm{d}v - \left\langle \mathbf{f}^{\mathsf{ext}}, \boldsymbol{\eta}\right\rangle \\ &+ \int_{\Omega}\big(\mathcal{W}'_{\mathsf{vol}}(\Theta) - p\big)\Xi\,J^{-1}\mathrm{d}v + \int_{\Omega} q(J-\Theta)\,J^{-1}\mathrm{d}v = 0, \quad \forall(\boldsymbol{\eta}, \Xi, q) \in V \times Q \times Q.\end{aligned} \tag{22}$$

4.1. Linearization

The variational formulation (22) is a non–linear problem in the unknowns $(\mathbf{u}, \Theta, p)$. We can devise two kinds of non–linearities: the first one is of constitutive nature, because $\mathsf{T}_{\mathsf{iso}}$ depends on the deformation $\boldsymbol{\varphi}$, as well as $\mathcal{W}_{\mathsf{vol}}$ depends on Θ; the second one is geometrical, because also the integration domain $\Omega = \boldsymbol{\varphi}(\Omega_0)$ is unknown.

The Newton's method is a classical iterative algorithm to find the solution of a non–linear problem. Given a generic operator $\mathcal{G}\colon W \to W^*$, where W is a Banach space and W^* its dual, the Newton's method to approximate $x \in W$ so that $\mathcal{G}(x) = 0$ reads as follows:

1. **Given** $x^0 \in W$
2. **Until** $\langle$convergence criteria$\rangle$ is satisfied:
3. **Solve for** δx such that $\mathrm{D}\mathcal{G}(x^k)\,\delta x = -\mathcal{G}(x^k)$
4. **Let** $x^{k+1} = x^k + \delta x$

(23)

The linear operator $\mathrm{D}\mathcal{G} \in \mathcal{L}(W, W^*)$ is the Gâteaux derivative of $\mathcal{G}$. As a convergence test, typically one checks that both the increment δx and the residual $\mathcal{G}(x_k)$ are smaller than a given tolerance, with respect to a suitable norm.

For our variational problem (22) we have $W = V \times Q \times Q$, $x = (\mathbf{u}, \Theta, p)$ and $\delta x = (\delta\mathbf{u}, \delta\Theta, \delta p)$. The computation of $\mathrm{D}\mathcal{G}(x_k)$ is just a tedious application of the chain–rule, so we simply report the final result:

$$\begin{aligned}\langle \mathrm{D}\mathcal{G}(x)\,\delta x, (\boldsymbol{\eta}, \Xi, p)\rangle = &\int_{\Omega}\Big(\nabla\delta\mathbf{u}\mathsf{T} + \big(\mathfrak{c}_{\mathsf{iso}} + p(\mathsf{I}\otimes\mathsf{I} - 2\mathbb{I})\big)\nabla\delta\mathbf{u} + \delta p\,\mathsf{I}\Big) : \nabla\boldsymbol{\eta}\,\mathrm{d}v \\ &+ \int_{\Omega}\Xi\left(\mathcal{W}''_{\mathsf{vol}}(\Theta)\delta\Theta - \delta p\right)J^{-1}\mathrm{d}v \\ &+ \int_{\Omega} q\left(\mathrm{div}\,\delta\mathbf{u} - J^{-1}\delta\Theta\right)\mathrm{d}v,\end{aligned} \tag{24}$$

where $\mathsf{c}_{\mathsf{iso}}$ is the spatial elasticity tensor of the isochoric term:

$$
\begin{aligned}
\mathsf{c}_{\mathsf{iso}} &= \mathbb{P} : \bar{\mathsf{c}}_{\mathsf{iso}} : \mathbb{P} + \frac{2}{3} J^{-1} \left(\operatorname{tr} \overline{\mathsf{T}}_{\mathsf{iso}}\right) \mathbb{P} - \frac{2}{3} \left(\operatorname{dev} \mathsf{T}_{\mathsf{iso}} \otimes \mathsf{I} + \mathsf{I} \otimes \operatorname{dev} \mathsf{T}_{\mathsf{iso}}\right), \\
\bar{\mathsf{c}}_{\mathsf{iso}} &= 4\widehat{\mathcal{W}}_1''(\mathcal{I}_1^{\mathsf{iso}})\, \mathsf{B}_{\mathsf{iso}} \otimes \mathsf{B}_{\mathsf{iso}} \\
&\quad + 4\widehat{\mathcal{W}}_{4,\mathbf{f}_\circ}''(\mathcal{I}_{4,\mathbf{f}_\circ}^{\mathsf{iso}})\, \mathbf{f}_{\mathsf{iso}} \otimes \mathbf{f}_{\mathsf{iso}} \otimes \mathbf{f}_{\mathsf{iso}} \otimes \mathbf{f}_{\mathsf{iso}} \\
&\quad + 4\widehat{\mathcal{W}}_{4,\mathbf{s}_\circ}''(\mathcal{I}_{4,\mathbf{s}_\circ}^{\mathsf{iso}})\, \mathbf{s}_{\mathsf{iso}} \otimes \mathbf{s}_{\mathsf{iso}} \otimes \mathbf{s}_{\mathsf{iso}} \otimes \mathbf{s}_{\mathsf{iso}} \\
&\quad + 4\widehat{\mathcal{W}}_{8,\mathbf{f}_\circ\mathbf{s}_\circ}''(\mathcal{I}_{8,\mathbf{f}_\circ\mathbf{s}_\circ}^{\mathsf{iso}})\, \operatorname{sym}(\mathbf{f}_{\mathsf{iso}} \otimes \mathbf{s}_{\mathsf{iso}}) \otimes \operatorname{sym}(\mathbf{f}_{\mathsf{iso}} \otimes \mathbf{s}_{\mathsf{iso}}).
\end{aligned}
$$

We have introduced the fourth–order tensor $\mathbb{I}$ such that $\mathbb{I}\mathsf{A} = \mathsf{A}$ for every second–order tensor A, and the tensor $\mathbb{P}$ as the linear application such that $\mathbb{P}\colon \mathsf{A} \mapsto \operatorname{dev} \mathsf{A}$:

$$
\mathbb{P} := \mathbb{I} - \frac{1}{3} \mathsf{I} \otimes \mathsf{I}.
$$

Even through the expression obtained above contains several terms, its mathematical structure is particularly simple. We can identify two contributions:

$$
\begin{aligned}
\int_\Omega \nabla \delta\mathbf{u} \mathsf{T} : \nabla \boldsymbol{\eta} \, \mathrm{d}v \quad &= \quad \text{residual geometrical contribution,} \\
\int_\Omega (\mathsf{c}_{\mathsf{iso}} + \mathsf{c}_{\mathsf{vol}}) \nabla \delta\mathbf{u} : \nabla \boldsymbol{\eta} \, \mathrm{d}v \quad &= \quad \text{constitutive contribution,}
\end{aligned}
$$

where $\mathsf{c}_{\mathsf{vol}} = p(\mathsf{I} \otimes \mathsf{I} - 2\mathbb{I})$ is spatial elasticity tensor associated to the volumetric part.

4.2. Galerkin formulation

Consider a finite dimensional subspace V_h of V and other two finite dimensional subspaces Q_h^p and Q_h^Θ of Q, where h stands for any discretization parameter (typically the size of the mesh). Then the Galerkin problem associated to the tangent problem reads as follows (see, e.g. Quarteroni (2014)):

Find $(\delta\mathbf{u}_h, \delta\Theta_h, \delta p_h) \in V_h \times Q_h^p \times Q_h^\Theta$ such that

$$
\begin{aligned}
&\int_\Omega \Big(\nabla \delta\mathbf{u}_h \mathsf{T} + \big(\mathsf{c}_{\mathsf{iso}} + \mathsf{c}_{\mathsf{vol}}\big)\big) \nabla \delta\mathbf{u}_h + \delta p_h \mathsf{I} \Big) : \nabla \boldsymbol{\eta}_h \, \mathrm{d}v = \left\langle \mathbf{f}^{\mathsf{ext}}, \boldsymbol{\eta}_h \right\rangle - \int_\Omega \mathsf{T} : \nabla \boldsymbol{\eta}_h \, \mathrm{d}v, \\
&\int_\Omega \Xi_h \left(\mathcal{W}_{\mathsf{vol}}''(\Theta) \delta\Theta_h - \delta p_h \right) J^{-1} \mathrm{d}v = \int_\Omega \Xi_h \left(p - \mathcal{W}_{\mathsf{vol}}'(\Theta) \right) J^{-1} \mathrm{d}v, \\
&\int_\Omega q_h \left(\operatorname{div} \delta\mathbf{u}_h - J^{-1} \delta\Theta_h \right) \mathrm{d}v = \int_\Omega q_h \left(1 - J^{-1}\Theta \right) \mathrm{d}v, \qquad \forall (\boldsymbol{\eta}_h, \Xi_h, q_h) \in V_h \times Q_h^p \times Q_h^\Theta.
\end{aligned}
$$

The discrete tangent problem can be rewritten in matrix form after introducing the bases $\{\boldsymbol{\Phi}_i\}_{i=1}^{N_v}$, $\{\Psi_i^p\}_{i=1}^{N_p}$ and $\{\Psi_i^\Theta\}_{i=1}^{N_\Theta}$ for the spaces V_h, Q_h^p and Q_h^Θ, respectively. In fact we have that:

$$
\delta\mathbf{u}_h(\mathbf{X}) = \sum_{i=1}^{N_{\mathsf{v}}} \delta u_h^i \, \boldsymbol{\Phi}_i(\mathbf{X}), \quad \delta\Theta_h(\mathbf{X}) = \sum_{i=1}^{N_p} \delta\Theta_h^i \, \Psi_i^p(\mathbf{X}), \quad \delta p_h(\mathbf{X}) = \sum_{i=1}^{N_\Theta} \delta p_h^i \, \Psi_i^\Theta(\mathbf{X}),
$$

where the coefficients form the vectors of the unknown $(\delta\mathbf{u}, \delta\boldsymbol{\Theta}, \delta\mathbf{p})$ with components

$$
\left[\delta\mathbf{u}_h\right]_i = \delta u_h^i, \qquad \left[\delta\boldsymbol{\Theta}_h\right]_i = \delta\Theta_h^i, \qquad \left[\delta\mathbf{p}_h\right]_i = \delta p_h^i.
$$

The algebraic form of the tangent problem is then:

$$
\text{Find } (\delta\mathbf{u}_h, \delta\boldsymbol{\Theta}_h, \delta\mathbf{p}_h) \text{ such that } \quad \begin{bmatrix} \mathsf{K}_{\varphi\varphi} & \mathsf{O} & \mathsf{K}_{\varphi\mathsf{p}} \\ \mathsf{O} & \mathsf{K}_{\theta\theta} & -\mathsf{K}_{\theta\mathsf{p}} \\ \mathsf{K}_{\mathsf{p}\varphi} & -\mathsf{K}_{\mathsf{p}\theta} & \mathsf{O} \end{bmatrix} \begin{bmatrix} \delta\boldsymbol{\varphi} \\ \delta\boldsymbol{\Theta} \\ \delta\mathbf{p} \end{bmatrix} = \begin{bmatrix} \mathbf{f}_\varphi \\ \mathbf{f}_\theta \\ \mathbf{f}_{\mathsf{p}} \end{bmatrix}. \tag{25}
$$

The matrix in (25) is symmetric. The explicit definition of its entries is:

$$
\begin{aligned}
\big[\mathsf{K}_{\varphi\varphi}\big]_{ij} &:= \int_\Omega \Big(\nabla\delta\boldsymbol{\Phi}_j\mathsf{T} + \big(\mathfrak{c}_{\mathsf{iso}} + p(\mathsf{I}\otimes\mathsf{I} - 2\mathbb{I})\big)\nabla\delta\boldsymbol{\Phi}_j\Big) : \nabla\boldsymbol{\Phi}_i \,\mathrm{d}v,\\
\big[\mathsf{K}_{\theta\theta}\big]_{ij} &:= \int_\Omega \mathcal{W}''_{\mathsf{vol}}(\Theta)\ \Psi_j^\Theta\Psi_i^\Theta\ J^{-1}\mathrm{d}v,\\
\big[\mathsf{K}_{\varphi\mathsf{p}}\big]_{ij} &:= \int_\Omega \Psi_j^p \operatorname{div}\boldsymbol{\Phi}_i \,\mathrm{d}v,\\
\big[\mathsf{K}_{\theta\mathsf{p}}\big]_{ij} &:= \int_\Omega \Psi_j^p\Psi_i^\Theta\ J^{-1}\mathrm{d}v,\\
\big[\mathbf{f}_\varphi\big]_i &:= \langle \mathbf{f}^{\mathsf{ext}}, \Phi_i\rangle - \int_\Omega \mathsf{T} : \nabla\boldsymbol{\Phi}_i \,\mathrm{d}v,\\
\big[\mathbf{f}_\theta\big]_i &:= \int_\Omega \Psi_i^\Theta\ \big(p - \mathcal{W}'_{\mathsf{vol}}(\Theta)\big)J^{-1}\mathrm{d}v,\\
\big[\mathbf{f}_\mathsf{p}\big]_i &:= \int_\Omega \Psi_i^p\ \big(1 - J^{-1}\Theta\big)\mathrm{d}v,
\end{aligned}
$$

Given a triangulation $\mathscr{T}_h$ of a polygonal approximation $\tilde{\Omega}_0$ of the domain Ω_0, the finite element spaces we are going to use are defined as follows:

$$
\begin{aligned}
\mathbb{CG}_p(\tilde{\Omega}_0) &:= \Big\{u \in \mathcal{C}(\tilde{\Omega}_0)\colon\ u|_K \text{ is a polynomial of degree } p, \text{ for } K \in \mathscr{T}_h\Big\},\\
\mathbb{DG}_p(\tilde{\Omega}_0) &:= \Big\{u \in \mathrm{L}^2(\tilde{\Omega}_0)\colon\ u|_K \text{ is a polynomial of degree } p, \text{ for } K \in \mathscr{T}_h\Big\},\\
\mathbb{B}_p(\tilde{\Omega}_0) &:= \Big\{b \in \mathrm{L}^2(\tilde{\Omega}_0)\colon\ b|_K \text{ is a polynomial of degree } p, \text{ with } b|_{\partial K} = 0, \text{ for } K \in \mathscr{T}_h\Big\}.
\end{aligned}
$$

On tetrahedral meshes we select $V_h = \big(\mathbb{CG}_1 \oplus \mathbb{B}_4\big)^3$ or $V_h = \big[\mathbb{CG}_2\big]^3$, $Q_h^p = \mathbb{CG}_1$ and $Q_h^\Theta = \mathbb{DG}_0$. These choices avoid locking and also guarantee a good accuracy of the solution. The discontinuous Galerkin approximation for the dilational variable makes it possible to easily invert the matrix $\mathsf{K}_{\theta\theta}$ element–wise and apply a static condensation.

The non–linear mechanical solver has been implemented with FEniCS (Logg et al., 2012), and then ported to LifeV (`http://www.lifev.org`). The meshes for the ventricle have been generated with Gmsh (Geuzaine and Remacle, 2009) and the solution is post–processed with Paraview (`http://www.paraview.org`) and other scripts. All the mentioned software are open–source and freely available on the internet, including the GNU/Linux operating system.

4.3. Boundary conditions

If $\partial_{\mathrm{D}}\Omega_0 = \varnothing$ or, more generally, if essential boundary conditions are applied only on some components of the deformation, the solution might not be unique: any rigid motion that satisfies the boundary conditions can be superimposed to the solution of the elastic problem. It follows, for instance, that the linear and angular momentum of the external loads (body force and surface traction) should balance, because otherwise the deformation cannot be static. On the other hand, even if a small[1] portion of the boundary is fixed, any force or momentum can be balanced by the constraint reaction.

As we shall see, it is not obvious to constrain the motion of the left ventricle in a physiologically correct way, even taking into account the surrounding anatomy of the heart, because the organ slightly moves and rotates during the heartbeat. Moreover, the heart is actually contained in a sac called pericardium, which is filled with a fluid and whose stiffness is rather high. This prevents extremely large displacements of the muscle. Our approach is then to constrain at a minimum the load free boundary conditions by two possible

[1] From a mathematical standpoint this means that the capacity of the portion of the boundary is not zero.

strategies: introduce a "small" portion of essential boundary or require zero mean rotation and zero mean displacement. A popular alternative is to prescribe a Robin–type boundary condition to mimic the presence of the pericardium and other elastic components surrounding the heart.

The former approach can be formulated as follows: a global constraint on the solution is enforced in order to avoid any rigid motion, such as

$$\int_{\Omega_0} \delta\mathbf{u}_h \, \mathrm{d}V = 0,$$

for the zero mean translation and, in a similar fashion, the condition

$$\int_{\Omega_0} \mathbf{X} \wedge \delta\mathbf{u}_h \, \mathrm{d}V = 0$$

for a zero mean rotation. For instance, a Lagrange formulation of problem (21) accounting for these constraints should be

$$\mathscr{L}(\mathbf{u}, \Theta, p, \mathbf{c}_1, \mathbf{c}_2) := \mathcal{F}_{\mathrm{HW}}(\mathbf{u}, \Theta, p) - \mathbf{c}_1 \cdot \int_{\Omega_0} \mathbf{u} \, \mathrm{d}V - \mathbf{c}_2 \cdot \int_{\Omega_0} \mathbf{X} \wedge \mathbf{u} \, \mathrm{d}V,$$

where we have two new unknowns $\mathbf{c}_1$, $\mathbf{c}_2 \in \mathbb{R}^3$ to be appended to the former set $(\mathbf{u}, \Theta, p)$.

5. Numerical assessment on a tissue slab

5.1. Compression with constant fibers distribution: a quasi–explicit solution

It is well known that simple shear is particularly difficult to obtain in large deformation regimes (Destrade et al., 2012), because of the so–called "Poynting effect": no simple shear in deformation can be produced by a simple shear in boundary conditions. In this specific test we produce simple shear by applying pure pressure on a cube of orthotropic material.

In this section we address the compression of a cube whose constant microstructure, in Cartesian coordinates, reads as follows:

$$\mathbf{f}_\circ = \cos\alpha \, \mathbf{e}_1 + \sin\alpha \, \mathbf{e}_2, \qquad \mathbf{s}_\circ = \mathbf{e}_3.$$

The fibers lie on planes orthogonal to $\mathbf{e}_3$, which also corresponds to the sheets direction, and they form an angle α with respect to the horizontal direction $\mathbf{e}_1$. A uniform compressive normal pressure p_{load} is applied to the faces orthogonal to $\mathbf{e}_3$ (see figure 2).

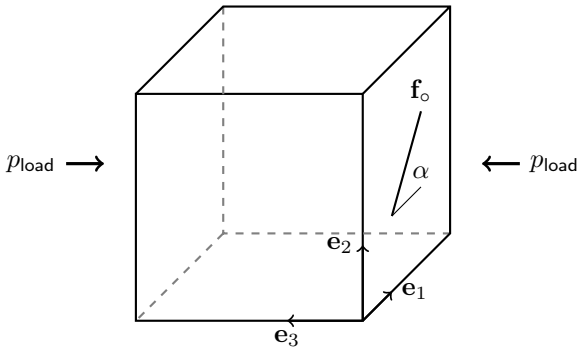

Figure 2: Reference geometry for the pressure–induced shear test, with constant microstructure.

The aim is to mimic the behavior of a small portion of the wall of the left ventricle when passively inflated. From a numerical viewpoint we want to establish whether our implementation correctly captures rotations, which is an important expected result, not trivial considering the complexity of the model. This test also represents a good benchmark for our solver when the tangent problem is singular (see section 4.3).

We look for an homogeneous deformation of the type

$$x = \lambda_1 X + \kappa\lambda_2 Y, \qquad y = \lambda_2 Y, \qquad z = \lambda_3 Z.$$

where the tensor gradient of deformation can be decomposed into an axial strain followed by a simple shear:

$$\mathsf{F} = \begin{bmatrix} 1 & \kappa & 0 \\ 0 & 1 & 0 \\ 0 & 0 & 1 \end{bmatrix} \begin{bmatrix} \lambda_1 & 0 & 0 \\ 0 & \lambda_2 & 0 \\ 0 & 0 & \lambda_3 \end{bmatrix} = \begin{bmatrix} \lambda_1 & \kappa\lambda_2 & 0 \\ 0 & \lambda_2 & 0 \\ 0 & 0 & \lambda_3 \end{bmatrix}. \tag{26}$$

Since the material is incompressible, $\lambda_3 = (\lambda_1\lambda_2)^{-1}$, thus the unknowns are λ_1, λ_2, κ and the pressure. The left and right Cauchy–Green tensors are

$$\mathsf{B} = \begin{bmatrix} \lambda_1^2 + \kappa^2\lambda_2^2 & \kappa\lambda_2^2 & 0 \\ \kappa\lambda_2^2 & \lambda_2^2 & 0 \\ 0 & 0 & (\lambda_1\lambda_2)^{-2} \end{bmatrix}, \qquad \mathsf{C} = \begin{bmatrix} \lambda_1^2 & \kappa\lambda_1\lambda_2 & 0 \\ \kappa\lambda_1\lambda_2 & (\kappa^2+1)\lambda_2^2 & 0 \\ 0 & 0 & (\lambda_1\lambda_2)^{-2} \end{bmatrix},$$

and the corresponding invariants are

$$\begin{aligned} \mathcal{I}_1 &= \operatorname{tr}\mathsf{C} = \lambda_1^2 + (\kappa^2+1)\lambda_2^2 + (\lambda_1\lambda_2)^{-2}, \\ \mathcal{I}_{4,\mathbf{f}_\circ} &= \mathbf{f}_\circ \cdot \mathsf{C}\mathbf{f}_\circ = (\lambda_1\cos\alpha + \kappa\lambda_2\sin\alpha)^2 + \lambda_2^2\sin^2\alpha, \\ \mathcal{I}_{4,\mathbf{s}_\circ} &= \mathbf{s}_\circ \cdot \mathsf{C}\mathbf{f}_\circ = (\lambda_1\lambda_2)^{-2}, \\ \mathcal{I}_{8,\mathbf{f}_\circ\mathbf{s}_\circ} &= \mathbf{s}_\circ \cdot \mathsf{C}\mathbf{f}_\circ = 0. \end{aligned}$$

The non–null components of the Cauchy stress tensor (7) read as follows:

$$\begin{aligned} \mathsf{T}_{11} &= 2\widetilde{\mathcal{W}}_1'(\mathcal{I}_1)(\lambda_1^2 + \kappa^2\lambda_2^2) + 2\widetilde{\mathcal{W}}_{4,\mathbf{f}_\circ}'(\mathcal{I}_{4,\mathbf{f}_\circ})(\lambda_1\cos\alpha + \kappa\lambda_2\sin\alpha)^2 - p, \\ \mathsf{T}_{22} &= 2\widetilde{\mathcal{W}}_1'(\mathcal{I}_1)\lambda_2^2 + 2\widetilde{\mathcal{W}}_{4,\mathbf{f}_\circ}'(\mathcal{I}_{4,\mathbf{f}_\circ})\lambda_2^2\sin^2\alpha - p, \\ \mathsf{T}_{33} &= 2\widetilde{\mathcal{W}}_1'(\mathcal{I}_1)(\lambda_1\lambda_2)^{-2} + 2\widetilde{\mathcal{W}}_{4,\mathbf{s}_\circ}'(\mathcal{I}_{4,\mathbf{s}_\circ})(\lambda_1\lambda_2)^{-2} - p, \\ \mathsf{T}_{12} = \mathsf{T}_{21} &= 2\widetilde{\mathcal{W}}_1'(\mathcal{I}_1)\kappa\lambda_2^2 + 2\widetilde{\mathcal{W}}_{4,\mathbf{f}_\circ}'(\mathcal{I}_{4,\mathbf{f}_\circ})(\lambda_1\cos\alpha + \kappa\lambda_2\sin\alpha)\lambda_2\sin\alpha. \end{aligned}$$

All the components of the Cauchy traction must vanish except $\mathsf{T}_{33} = -p_{\mathsf{load}}$. Since the deformation keeps the faces orthogonal to $\mathbf{e}_2$ still orthogonal, we have $\mathsf{T}_{22} = 0$. Moreover, the remaining two faces become orthogonal to $\mathbf{e}_1 - \kappa\mathbf{e}_2$, thus we impose null normal and tangent stress as follows:

$$\begin{aligned} (\mathbf{e}_1 - \kappa\mathbf{e}_2)\cdot\mathsf{T}(\mathbf{e}_1 - \kappa\mathbf{e}_2) &= \mathsf{T}_{11} - 2\kappa\mathsf{T}_{12} + \kappa^2\mathsf{T}_{22} = 0, \\ (\kappa\mathbf{e}_1 + \mathbf{e}_2)\cdot\mathsf{T}(\mathbf{e}_1 - \kappa\mathbf{e}_2) &= \kappa\mathsf{T}_{11} + (1-\kappa^2)\mathsf{T}_{12} - \kappa\mathsf{T}_{22} = 0. \end{aligned}$$

The pressure can be easily computed from the equation $\mathsf{T}_{22} = 0$:

$$p = 2\widetilde{\mathcal{W}}_1'(\mathcal{I}_1)\lambda_2^2 + 2\widetilde{\mathcal{W}}_{4,\mathbf{f}_\circ}'(\mathcal{I}_{4,\mathbf{f}_\circ})\lambda_2^2\sin^2\alpha,$$

which leaves us the following non–linear system of 3 equations in the unknowns (λ_1, λ_2, κ):

$$\begin{cases} \widetilde{\mathcal{W}}_1'(\mathcal{I}_1)\Big(\lambda_1^2 + (\kappa^2-1)\lambda_2^2\Big) + \widetilde{\mathcal{W}}_{4,\mathbf{f}_\circ}'(\mathcal{I}_{4,\mathbf{f}_\circ})\Big((\lambda_1\cos\alpha + \kappa\lambda_2\sin\alpha)^2 - \lambda_2^2\sin^2\alpha\Big) = 0, \\ \widetilde{\mathcal{W}}_1'(\mathcal{I}_1)\Big((\lambda_1\lambda_2)^{-2} - \lambda_2^2\Big) + \widetilde{\mathcal{W}}_{4,\mathbf{s}_\circ}'(\mathcal{I}_{4,\mathbf{s}_\circ})(\lambda_1\lambda_2)^{-2} - \widetilde{\mathcal{W}}_{4,\mathbf{f}_\circ}'(\mathcal{I}_{4,\mathbf{f}_\circ})\lambda_2^2\sin^2\alpha = -\tfrac{1}{2}p_{\mathsf{load}}, \\ \widetilde{\mathcal{W}}_1'(\mathcal{I}_1)\kappa\lambda_2 + \widetilde{\mathcal{W}}_{4,\mathbf{f}_\circ}'(\mathcal{I}_{4,\mathbf{f}_\circ})(\lambda_1\cos\alpha + \kappa\lambda_2\sin\alpha)\sin\alpha = 0. \end{cases} \tag{27}$$

The non–linear form of (27) prevents an explicit determination of the unknowns, but the algebraic system can be easily solved numerically. Nonetheless, it is possible to observe some interesting features of the solution, also supported by simulations.

- κ and α have opposite sign; indeed, from the third equation of (27), we have

$$\kappa \underbrace{\lambda_2 \left(\mathcal{W}_1'(\mathcal{I}_1) + \mathcal{W}_{4,\mathbf{f}_\circ}'(\mathcal{I}_{4,\mathbf{f}_\circ}) \sin^2\alpha\right)}_{\geq 0} = -\mathcal{W}_{4,\mathbf{f}_\circ}'(\mathcal{I}_{4,\mathbf{f}_\circ})\lambda_1 \cos\alpha \sin\alpha.$$

  In particular κ is zero for $\alpha \in \left\{-\frac{\pi}{2}, 0, \frac{\pi}{2}\right\}$, and it is maximum (resp. minimum) for $\alpha = \mp\frac{\pi}{4}$, as follows from symmetry arguments too.

- $\mathcal{I}_{4,\mathbf{f}_\circ}$ is everywhere greater than one, thus fibers are under tension. Indeed, if $\mathcal{I}_{4,\mathbf{f}_\circ} < 1$, we would have $\kappa = 0$, so $\lambda_1 = \lambda_2$, but this would not be consistent with the second equation in (27) unless $p_{\mathsf{load}} < 0$, i.e. when the cube is under traction. This shows a clear asymmetry between the two cases: shear is observed only when the cube is compressed.

  A similar argument can then be applied to $\mathcal{I}_{4,\mathbf{s}_\circ}$, proving that sheets are always in compressive regime and thus $\mathcal{W}_{4,\mathbf{s}_\circ}$ doesn't show up. This observation, with $\mathcal{I}_{8,\mathbf{f}_\circ\mathbf{s}_\circ} = 0$ implies that in this test the model behaves as a transversely isotropic one, so that the deformation is essentially dictated by the fibers elongation.

5.2. Compression with variable fibers distribution

An interesting aspect of cardiac mechanics is that the fiber angle α (defined in the previous section) is not fixed across the wall, and it significantly varies between the two sides (LeGrice et al., 2001). Consider the following microstructure (see figure 3):

$$\mathbf{f}_\circ = \cos\alpha(Z)\,\mathbf{e}_1 + \sin\alpha(Z)\,\mathbf{e}_2, \qquad \mathbf{s}_\circ = \mathbf{e}_3,$$

where, in this case, α depends on the Z (transmural) coordinate as follows:

$$\alpha(Z) = \alpha_0\,(0.5 - Z) + \alpha_1\,(0.5 + Z),$$

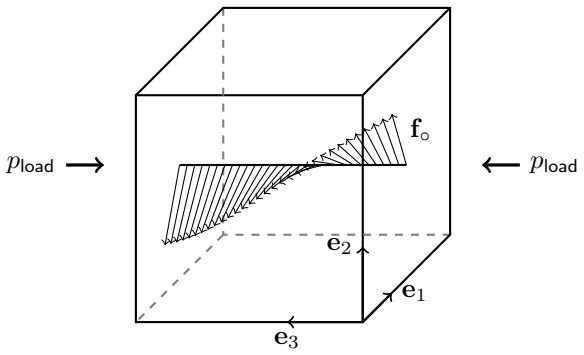

Figure 3: Reference geometry of the pressure–induced shear test with variable microstructure.

The expected deformation is not uniform but spatially dependent, especially in the Z–direction, and results in a geometrically simple but kinematically complex benchmark to test the numerical convergence. Here we purposely make use of a tetrahedral (and not hexahedral) mesh, in order to better understand the effect of the mesh on the solution, in terms of error on the strain and the stress. This is done keeping in mind that producing a tetrahedral mesh for a patient–specific geometry of the ventricle (or possibly of both ventricles), is much easier than an hexahedral one.

We perform a large number of tests with different combinations of material parameters, boundary conditions, and fibers distribution, plotting several quantities of interest, such as the invariants and the stress,

along the segment $(0, 0, z)$, with $z \in [-0.5, 0.5]$. We also measure the torsion τ as the angle between the projection on the $\mathbf{e}_1$–$\mathbf{e}_2$ plane of $\mathbf{X}$ and $\mathbf{x} = \mathbf{X} + \mathbf{u}$:

$$\sin\tau = \frac{\overline{\mathbf{X}} \wedge \overline{\mathbf{x}}}{\|\overline{\mathbf{X}}\|\|\overline{\mathbf{x}}\|} \cdot \mathbf{e}_1, \qquad \overline{\mathbf{X}} = \mathbf{X} - (\mathbf{X} \cdot \mathbf{e}_1)\,\mathbf{e}_1, \quad \overline{\mathbf{x}} = \mathbf{x} - (\mathbf{x} \cdot \mathbf{e}_1)\,\mathbf{e}_1.$$

The torsion is sampled along the segment $(0, 0.5, z)$.

The final deformation can be intuitively understood as a superposition of different in–plane shear deformations. Indeed, we know from the previous section that when the fiber angle is constant, the whole cube is deformed into a prism with rhomboid section; in the present case, we can suppose that every section, which has its own fiber direction, is deformed into a rhombus as well, but with an opening angle that depends on the fiber angle. The whole deformation is approximatively obtained piling all these sections.

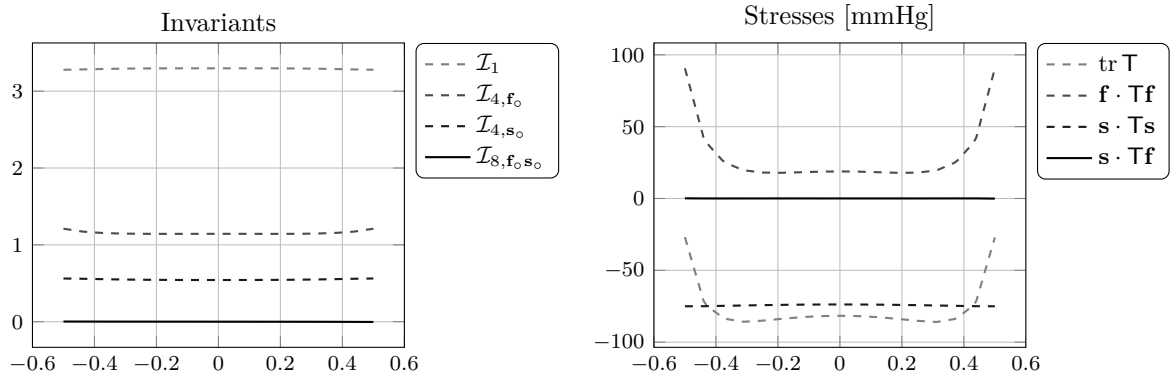

Figure 4: Invariants and components of the Cauchy stress T with respect to z–coordinate of the pressure–induced shear test with variable fiber microstructure.

This intuitive sketch is confirmed by the fact that $\mathcal{I}_{8,\mathbf{f}_\circ\mathbf{s}_\circ}$ is very small (fig. 4), so the sections orthogonal to $\mathbf{e}_1$ do not change orientation and $\mathcal{I}_{4,\mathbf{s}_\circ}$ doesn't vary that much across the cube, and its value is comparable to the one obtained with constant fiber direction. Also the torsion smoothly varies from $-5°$ to $5°$.

We performed a set of simulations to inspect different choices of fibers distribution (fig. 5). The reference case is a constant fiber direction parallel to $\mathbf{e}_1$, which is a uniform axial compression along $\mathbf{e}_3$. Surprisingly, the displacement in the $\mathbf{e}_3$ direction is not significantly affected by the fiber distribution while, as expected, the most prominent dissimilarity is in the torsion, absent in the reference case. Concerning the stress, the component along $\mathbf{f}$ significantly increases with the fiber angle variability, especially at the boundaries.

Finally, we also considered an asymmetric distribution of the fibers, as assumed by some authors for the left ventricle. The loss of symmetry is highlighted also by the value of the fibers invariant and the corresponding stress, but the mean values is comparable to the symmetric case. On the other hand, the torsion is quite different: in this case one side rotates less than in the other one, and the total variation is less than the $\pm\frac{\pi}{3}$ case. We find that no apparent difference between a variable and constant fibers distribution exists in terms of strain and stress. The most significant difference is in the torsion, which is however a major indicator of functionality in cardiovascular physiology.

The analysis of the deformation clearly suggests that the sheet–specific strain energy contribution $\mathcal{W}_{4,\mathbf{s}_\circ}$ is always zero and that $\mathcal{W}_{8,\mathbf{f}_\circ\mathbf{s}_\circ}$ is negligible, because $\mathcal{I}_{8,\mathbf{f}_\circ\mathbf{s}_\circ} \approx 0$. For the proof, we consider a modified model where these two terms are explicitly removed, going from an orthotropic to a transversely isotropic model.

The conclusion we draw is that for this passive mechanics test it is not worth using an orthotropic model because a transversely isotropic one is sufficient to capture the essential mechanics. This is also implicitly stated by the model itself, because the condition

$$\mathcal{W}_{4,\mathbf{s}_\circ} > 0 \qquad \Leftrightarrow \qquad \mathcal{I}_{4,\mathbf{s}_\circ} > 1$$

behaves as a switch that reduces the model under specific deformation regimes.

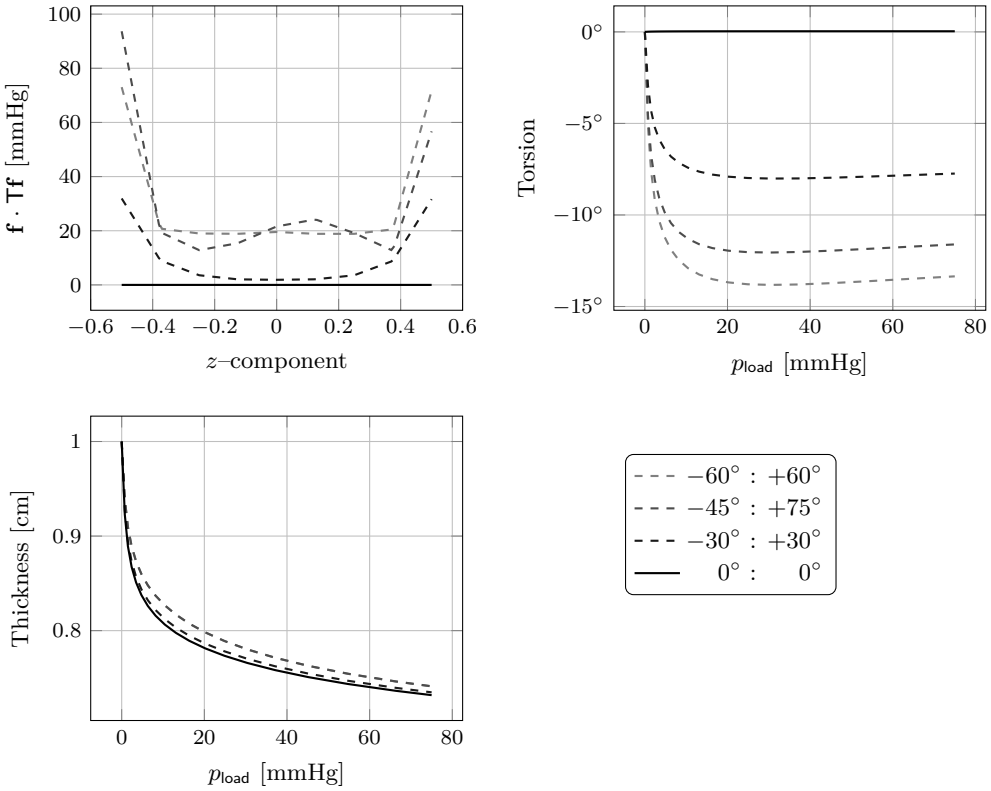

Figure 5: Fiber angle sensitivity of the fiber stress, torsion and thickness for the pressure–induced shear test with variable fiber microstructure.

5.3. Active contraction

The second set of tests consists in the active deformation of a traction–free elastic cube with variable fiber direction (see figure 3), using the active deformation form given in (20).

The gross deformation is that every slice of the cube with a given fiber angle undergoes a shear deformation depending on the fiber direction; since the variation of the angle is smooth, also the shear varies smoothly across the slices. On the other hand, integrity of the material requires a further elastic deformation and corresponding elastic energy storage. Figure 6 shows the final deformation for different values of γ (no shortening, 10% and 20%).

The convergence analysis is very similar to the one obtained for the passively compressed cube. With $N = 4$ subdivisions of each side of the cube we have convergence of the displacement and the torsion, and a good approximation of the stress, expect for $\mathcal{I}_{8,\mathbf{f}_\circ\mathbf{s}_\circ}$.

In this unloaded activation test, with very weak constrains at the boundary, all the components of the stress are very small (fig. 7): indeed, the order of magnitude of its highest component is 10^{-2} N/cm^2. This suggests that the final configuration is only slightly incompatible, hence $\mathsf{F} \approx \mathsf{F}_\mathsf{a}^{-1}$. More in particular, the greater the interval spanned by α, the greater the residual stress in the sheet direction.

The thickening of the tissue slab (fig. 8), which is measured in the direction of the sheets, does not significantly vary for the tested different fibers distribution. Since fibers and sheets remain orthogonal during the activation process, the invariant $\mathcal{I}_{4,\mathbf{s}_\circ}$ simply compensates the cross–area variation due to the fibers contraction, which is proportional to $(1-\gamma)^{-1}$, whatever the fiber distribution is.

In contrast with the results of the previous section, here the contribution to the strain energy provided by the elongation of the sheets $\mathcal{W}_{4,\mathbf{s}_\circ}$ is not null, since $\mathcal{I}^{\mathsf{e}}_{4,\mathbf{s}_\circ} > 1$. When $\mathcal{W}_{4,\mathbf{s}_\circ}$ is removed from the strain energy, several components of the strain take totally different values. On the other hand, the influence of

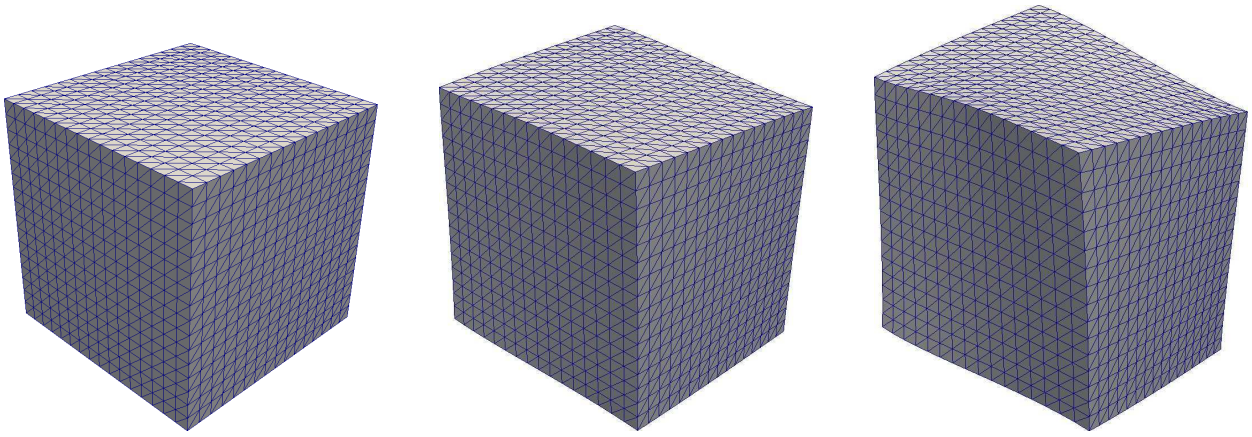

(a) $\gamma = 0.0$. (b) $\gamma = 0.1$. (c) $\gamma = 0.2$.

Figure 6: Activation of a cube with variable fiber direction ($\pm 60°$), with traction–free boundary conditions and material parameters from Wang et al. (2013b).

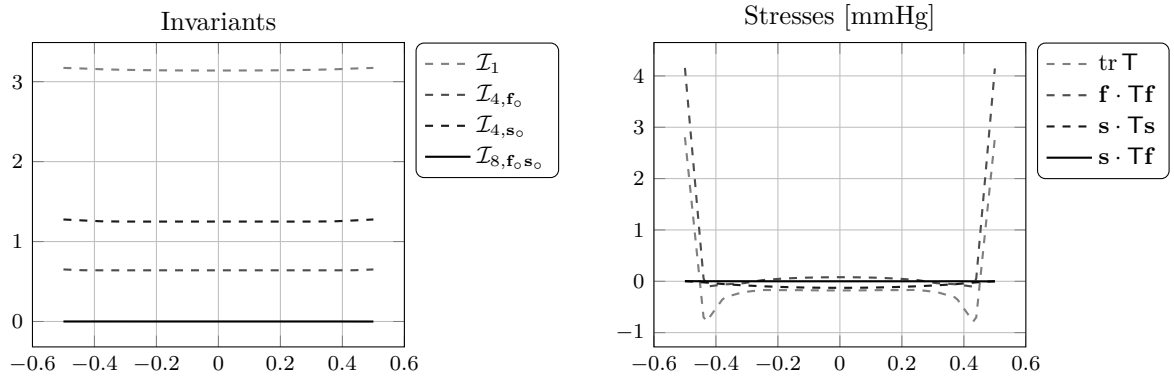

Figure 7: Invariants and Cauchy stress for the active contraction of a cube with variable fiber microstructure.

the eighth invariant $\mathcal{I}_{8,\mathbf{f}_\circ\mathbf{s}_\circ}$ remains negligible.

The convergence of the Newton scheme is strongly affected by several factors: with the material parameters from Holzapfel and Ogden (2009), the relaxation parameter needs to be an order of magnitude than using the material parameters proposed in Wang et al. (2013b), increasing ten times the total number of steps (146 versus 20). This is due to the strong difference in the isotropic shear modulus between the two data sets, take makes the material particularly soft in the fiber direction in the former case, since these are under compression ($\mathcal{I}^{\mathsf{e}}_{4,\mathbf{f}_\circ} < 1$) and therefore $\mathcal{W}_{4,\mathbf{f}_\circ} = 0$.

Concerning the Newton sub–iterations, we found that the simple switch-off of the fiber– and sheet–specific strain energy terms in contractile regime, has a negative impact on the convergence rate. In practice, we observe that the number of iterations needed for convergence grows when the activation of fibers is turned off. We argue that the convergence rate deteriorates because the second derivative of the strain energy function becomes discontinuous at $\mathsf{F} = \mathsf{I}$, and the quadratic convergence of the Newton solver is compromised, especially when the elastic deformation F_{e} is close to the identity, like in this case. This issue might be addressed by means of a mollifier, smoothing down the discontinuity.

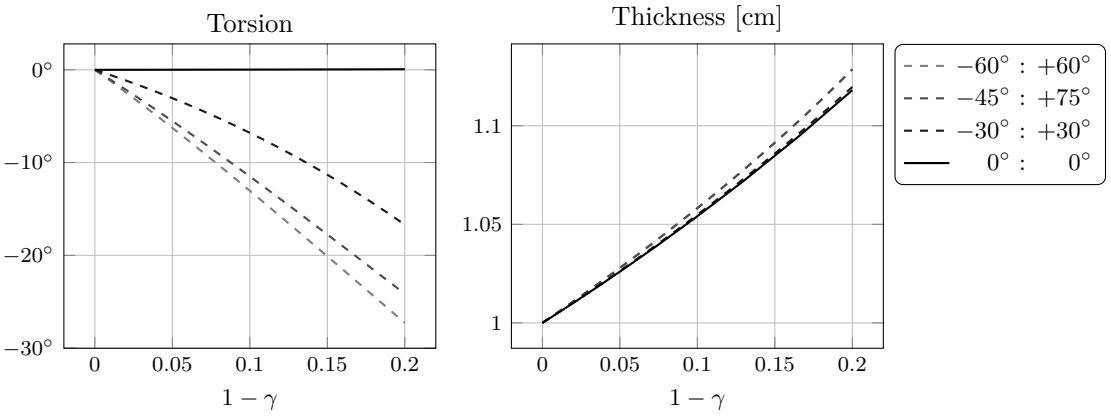

Figure 8: Fiber angle sensitivity of torsion and thickness of an activated cube.

6. Muscular thin films

In the previous sections we have discussed the performance of an active strain numerical model for a slab of orthotropic elastic material. While the theoretical and numerical results demonstrate the stability and fast convergence features of the algorithm, it remains to prescribe a rationale to fix the parameter γ, that dictates the contraction.

Recently, Feinberg et al. (2007) were able to build micro–actuators with myocytes, providing experimental data that perfectly fit our purpose, to evaluate γ in a controlled system with a collective dynamics of cells. These actuators, called muscular thin films (MTFs), are a combination of a polydimethylsiloxane substrate (PDMS) and rat ventricular cardiomyocytes, cultured on top of the former. The seeding face of the substrate can be engineered in order to have high/low nutrients density strips, aligned according to a specific direction. During the maturation, this external matrix induces a strong anisotropy in the tissue architecture (cfr. figure 9a).

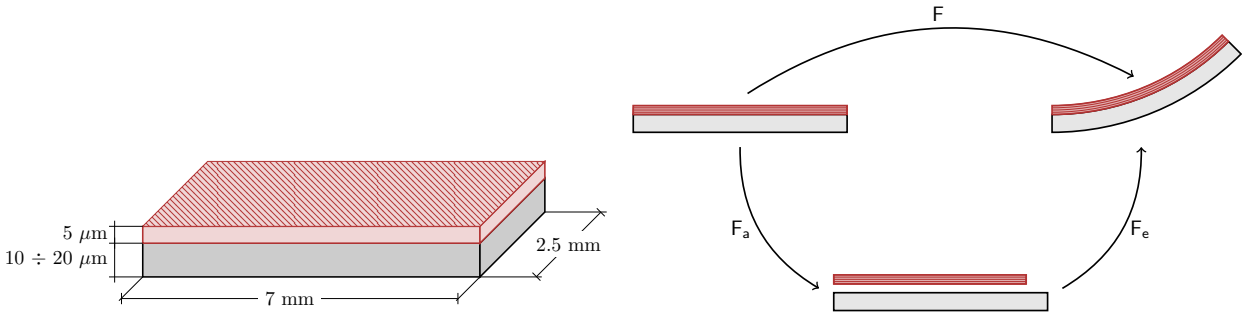

(a) Sketch of the geometry.

(b) Strain decomposition.

Figure 9: Muscular Thin Film (MTF).

The substrate is a thin sample of elastic material, and its mechanical properties are known with high accuracy (Shim et al., 2012). After maturation, the myocytes are able to produce a visible (and easily measurable) bending of the substrate during the contraction (systole), thanks to the active force exerted by the cells. The maximum observed curvature is therefore a function of few physical parameters. In our active strain hyperelastic framework the only unknown of the system is the contractility γ, which can therefore be evaluated by solving an inverse problem.

6.1. A specific model

Define the active strain tensor as follows:

$$\mathsf{F_a}(\mathbf{X},t)=\begin{cases}\mathsf{I}, & \text{for } \mathbf{X}\in \text{substrate},\\ (1-\gamma(t))\mathbf{f}_\circ\otimes\mathbf{f}_\circ+\frac{1}{\sqrt{1-\gamma(t)}}(\mathsf{I}-\mathbf{f}_\circ\otimes\mathbf{f}_\circ), & \text{for } \mathbf{X}\in \text{tissue}.\end{cases} \tag{28}$$

A sketch of the expected deformation according to our framework is presented in figure 9b. The activation $\mathsf{F_a}$ of equation (28) is a shortening of the tissue while keeping the substrate unchanged; the intermediate configuration cannot be compatible, since it is not possible to glue the tissue and the substrate together without an elastic deformation. Compatibility is provided by $\mathsf{F_e}$.

The strain energy density function is the sum of two contributions, one for the tissue, the other for the substrate

$$\mathcal{W}(\mathsf{F_e})=\mathcal{W}_{\mathsf{substrate}}(\mathsf{F_e})+\mathcal{W}_{\mathsf{tissue}}(\mathsf{F_e}).$$

More specifically, we assume that both the terms models a quasi–incompressible neo–Hookean material, with different shear and bulk moduli. The passive behavior of the fibers is neglected here. Resuming, we have the following strain energy:

$$\mathcal{W}(\mathsf{F})=\frac{\mu}{2}(\mathcal{I}_1^{\mathsf{iso}}-3)+\frac{\kappa}{4}(J^2-1-2\ln J),\qquad \begin{aligned}&\mu_{\mathsf{tissue}}=30\text{ kPa}, &&\mu_{\mathsf{substrate}}=1.5\text{ MPa},\\ &\kappa_{\mathsf{tissue}}=3\text{ MPa}, &&\kappa_{\mathsf{substrate}}=1.5\text{ GPa}.\end{aligned}$$

The most significant value is the shear modulus of the substrate, which is directly related to the curvature: the higher $\mu_{\mathsf{substrate}}$, the lower the curvature of the MTF.

6.2. Results

The numerical approximation of the bending problem introduces various difficulties to be addressed:

- large aspect–ratio of geometry;
- quasi–incompressibility of the materials;
- very different passive properties between the substrate and the tissue;
- discontinuous tangential stress across the interface.

In our case, we adopt a simple "monolithic" strategy, where both the elastic problems are solved simultaneously.

It is well known that for a bending problem the mesh needs to be very refined in the longitudinal direction; since this dimension is hundreds of times the thickness, we tested different meshes in order to understand which aspect ratio keeps a good accuracy of solution. With quadratic finite element, we found that $128 \div 512$ subdivisions of the longitudinal direction and $8 \div 16$ along the thickness is fine enough to achieve convergence to a mesh–independent solution.

Concerning the boundary conditions, we fix the displacement to zero at the bottom line of left face, and we apply symmetry condition to the left and the back face, i.e. no displacement is allowed along in the orthogonal direction.

						Avg.
ζ	0.207	0.227	0.244	0.284	0.324	0.257
γ	0.118	0.090	0.128	0.155	0.128	0.124

Table 1: Data from the experiments performed by Shim et al. (2012), with substrate thickness of 14.5 μm and the corresponding fitted values of γ for the activation.

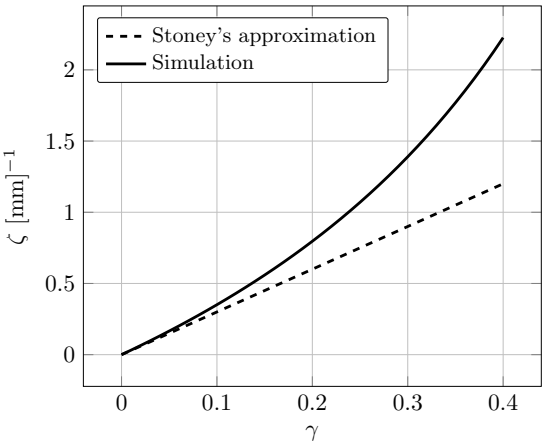

(a) Curvature vs. activation.

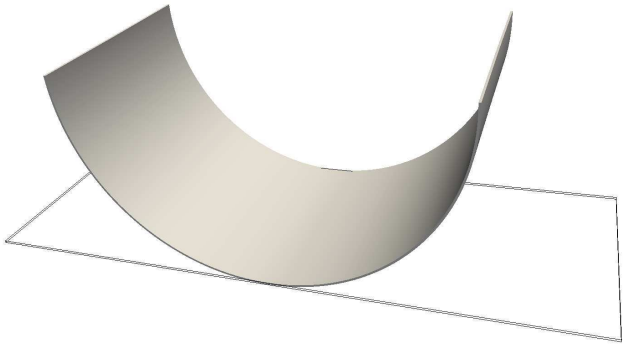

(b) Solution at $\gamma = 0.2$.

Figure 10: Simulation of a MTF with thickness of substrate of 18.0 μm.

Figure 10b shows the values of the final deformation for a 20% shortening of the myocytes; moreover, on the left panel we plot the curvature of the MTF[2] versus activation: for small deformations there is a good accordance with the Stoney's equation, while for large ones the thin film bends more than its linear counterpart.

Experimental data, taken from Shim et al. (2012), can be found in table 1. The authors perform several experiments, for different thickness of the substrate, and they measure the curvature. Here we match the curvature with the corresponding activation γ, which ranges between about 0.15 to 0.1, with an average of 0.124. This would suggest a physiological shortening range of about 10% to 15%, which is compatible with the experiments on isolated myocytes, or just a slightly lower than expected. However, in this context the fibers are not pre–stretched, so it is reasonable to conjecture that the working range of γ in the beating heart is higher.

Concluding remarks

An implementation of the Holzapfel–Ogden model in a finite element code that owns a number of mathematical and numerical positive features has been illustrated in detail. The contractile ability of the living material has been accounted for an active strain approach. In particular, we have critically addressed some issues that are sometimes overlooked in the literature: the codification of the active contraction in the model, the explicit calculation of the tangent problem, the efficient implementation of boundary conditions. The numerical code is then tested in a novel benchmark of homogeneous (non–trivial) deformation, for which we provide an exact explicit solution up to an algebraic equation. The same test case where the distribution of the fibers orientation is variable in space highlights the role of the fibers in dictating the cardiac rotation.

Our numerical results show that that the convexity of the strain energy, preserved by the active strain approach, conjugated with a three fields formulation ensure a very robust numerical scheme, converging in few Newton iterations while preserving the incompressibility of the deformation. The robustness and accuracy of the scheme is preserved when adopting different kind of finite elements, as allowed by the flexibility of the implementation.

In the considered test cases, which are a preliminary step to the simulation of a cardiac chamber, not all the strain energy terms retained by Holzapfel and Ogden play a relevant role, suggesting that the $\mathcal{I}_{8,\mathbf{f}_\circ\mathbf{s}_\circ}$ invariant could be even neglected from the beginning. We remark that our conclusion is just based on a

[2]The curvature is computed taking the inverse of the radius of the circle passing through three points at $x = 0$, $\frac{L}{2}$ and L.

preliminary test and could be modified at the light of numerical simulations of the left ventricle, for instance, when a more complicated kinematics occurs.

The active bending of an activated monolayer of cardiomyocytes is correctly reproduced and confirms the ability of the scheme to deal with strong geometric aspect ratios and very large deformations, while providing a range of activation parameters γ to be used in complex cardiac simulations.

Acknowledgments

This work has been supported by the European Research Council grant *Mathcard* (Mathematical Modelling and Simulation of the Cardiovascular System).

References

G. A. Holzapfel, R. W. Ogden, Constitutive modelling of passive myocardium: a structurally based framework for material characterization, Philosophical Transactions of the Royal Society A: Mathematical, Physical and Engineering Sciences 367 (1902) (2009) 3445–3475.

S. Göktepe, S. Acharya, J. Wong, E. Kuhl, Computational modeling of passive myocardium, International Journal for Numerical Methods in Biomedical Engineering 27 (1) (2011) 1–12.

H. Wang, X. Luo, H. Gao, R. Ogden, B. Griffith, C. Berry, T. Wang, A modified Holzapfel-Ogden law for a residually stressed finite strain model of the human left ventricle in diastole, Biomechanics and modeling in mechanobiology (2013a) 1–15.

H. Wang, H. Gao, X. Luo, C. Berry, B. Griffith, R. Ogden, T. Wang, Structure-based finite strain modelling of the human left ventricle in diastole, International journal for numerical methods in biomedical engineering 29 (1) (2013b) 83–103.

F. Nobile, A. Quarteroni, R. Ruiz-Baier, An active strain electromechanical model for cardiac tissue, International Journal for Numerical Methods in Biomedical Engineering 28 (1) (2012) 52–71.

S. Rossi, R. Ruiz-Baier, L. F. Pavarino, A. Quarteroni, Orthotropic active strain models for the numerical simulation of cardiac biomechanics, International Journal for Numerical Methods in Biomedical Engineering 28 (6-7) (2012) 761–788.

M. Böl, S. Reese, K. K. Parker, E. Kuhl, Computational modeling of muscular thin films for cardiac repair, Computational Mechanics 43 (4) (2009) 535–544.

P. W. Alford, A. W. Feinberg, S. P. Sheehy, K. K. Parker, Biohybrid thin films for measuring contractility in engineered cardiovascular muscle, Biomaterials 31 (13) (2010) 3613–3621.

T. J. Hughes, J. E. Marsden, Mathematical foundations of elasticity, Dover Publications, 1994.

S. S. Antman, Nonlinear problems of elasticity, vol. 107, Springer, 2005.

I.-S. Liu, On representations of anisotropic invariants, Int. J. Engng. Sci. 20 (10) (1982) 1099–1109.

M. Shariff, Nonlinear Orthotropic Elasticity: Only Six Invariants are Independent, Journal of Elasticity 110 (2) (2013) 237–241.

J. Merodio, R. Ogden, The influence of the invariant I8 on the stress–deformation and ellipticity characteristics of doubly fiber-reinforced non-linearly elastic solids, International Journal of Non-Linear Mechanics 41 (4) (2006) 556–563.

F. Yin, C. Chan, R. M. Judd, Compressibility of perfused passive myocardium, American Journal of Physiology-Heart and Circulatory Physiology 271 (5) (1996) H1864–H1870.

J. C. Simo, R. L. Taylor, Quasi-incompressible finite elasticity in principal stretches. Continuum basis and numerical algorithms, Computer Methods in Applied Mechanics and Engineering 85 (3) (1991) 273–310.

J. Schröder, P. Neff, Invariant formulation of hyperelastic transverse isotropy based on polyconvex free energy functions, International Journal of Solids and Structures 40 (2) (2003) 401–445.

T. Wakatsuki, M. S. Kolodney, G. I. Zahalak, E. L. Elson, Cell mechanics studied by a reconstituted model tissue, Biophysical Journal 79 (5) (2000) 2353–2368.

G. Iribe, M. Helmes, P. Kohl, Force-length relations in isolated intact cardiomyocytes subjected to dynamic changes in mechanical load, American Journal of Physiology-Heart and Circulatory Physiology 292 (3) (2007) H1487–H1497.

T. Usyk, R. Mazhari, A. McCulloch, Effect of laminar orthotropic myofiber architecture on regional stress and strain in the canine left ventricle, Journal of elasticity and the physical science of solids 61 (1-3) (2000) 143–164.

J. Aguado-Sierra, A. Krishnamurthy, C. Villongco, J. Chuang, E. Howard, M. J. Gonzales, J. Omens, D. E. Krummen, S. Narayan, R. C. Kerckhoffs, et al., Patient-specific modeling of dyssynchronous heart failure: a case study, Progress in biophysics and molecular biology 107 (1) (2011) 147–155.

W. K. Weiwad, W. A. Linke, M. H. Wussling, Sarcomere length–tension relationship of rat cardiac myocytes at lengths greater than optimum, Journal of molecular and cellular cardiology 32 (2) (2000) 247–259.

M. Baker, J. Ericksen, Inequalities restricting the form of the stress-deformation relations for isotropic elastic solids and Reiner-Rivlin fluids, J. Wash. Acad. Sci 44 (1954) 33–35.

D. Ambrosi, S. Pezzuto, Active stress vs. active strain in mechanobiology: constitutive issues, Journal of Elasticity 107 (2) (2012) 199–212.

M. Boyett, J. Frampton, M. Kirby, The length, width and volume of isolated rat and ferret ventricular myocytes during twitch contractions and changes in osmotic strength, Experimental physiology 76 (2) (1991) 259–270.

A. Quarteroni, Numerical Models for Differential Problems, Springer, 2nd edn., 2014.

A. Logg, K.-A. Mardal, G. Wells, Automated solution of differential equations by the finite element method: The fenics book, vol. 84, Springer, 2012.

C. Geuzaine, J.-F. Remacle, Gmsh: A 3-D finite element mesh generator with built-in pre-and post-processing facilities, International Journal for Numerical Methods in Engineering 79 (11) (2009) 1309–1331.
M. Destrade, J. G. Murphy, G. Saccomandi, Simple shear is not so simple, International Journal of Non-Linear Mechanics 47 (2) (2012) 210–214.
I. LeGrice, P. Hunter, A. Young, B. Smaill, The architecture of the heart: a data–based model, Philosophical Transactions of the Royal Society of London. Series A: Mathematical, Physical and Engineering Sciences 359 (1783) (2001) 1217–1232.
A. W. Feinberg, A. Feigel, S. S. Shevkoplyas, S. Sheehy, G. M. Whitesides, K. K. Parker, Muscular thin films for building actuators and powering devices, Science 317 (5843) (2007) 1366–1370.
J. Shim, A. Grosberg, J. C. Nawroth, K. Kit Parker, K. Bertoldi, Modeling of cardiac muscle thin films: pre-stretch, passive and active behavior, Journal of biomechanics 45 (5) (2012) 832–841.

MOX Technical Reports, last issues

Dipartimento di Matematica "F. Brioschi",
Politecnico di Milano, Via Bonardi 9 - 20133 Milano (Italy)

45/2014 Pezzuto, s.; Ambrosi,D.; Quarteroni, A.
An orthotropic active-strain model for the myocardium mechanics and its numerical approximation

44/2014 Pezzuto, s.; Ambrosi,D.
Active contraction of the cardiac ventricle and distortion of the microstructural architecture

43/2014 Brugiapaglia, S.; Micheletti, S.; Perotto, S.
Compressed solving: a numerical approximation technique for PDEs based on compressed sensing

42/2014 Canale, A.; Vantini, S.
Constrained Functional Time Series: an Application to Demand and Supply Curves in the Italian Natural Gas Balancing Platform

41/2014 Esfandiar, B.; Porta, G.; Perotto, S.; Guadagnini, A.
Impact of space-time mesh adaptation on solute transport modeling in porous media

40/2014 Antonietti, P.F.; Mazzieri, I.; Quarteroni, A.
Improving seismic risk protection through mathematical modeling

39/2014 Ghiglietti, A.; Paganoni, A.M.
Statistical inference for functional data based on a generalization of Mahalanobis distance

38/2014 Shen, H.; Truong, Y.; Zanini, P.
Independent Component Analysis for Spatial Stochastic Processes on a Lattice

37/2014 Giuliani, N.; Mola, A.; Heltai, L.; Formaggia,L.
FEM SUPG stabilisation of mixed isoparametric BEMs: application to linearised free surface flows

36/2014 Abb,A.;Bonaventura,L.; Nini, M.;Restelli,M.;
Anisotropic dynamic models for Large Eddy Simulation of compressible flows with a high order DG method